



Durham E-Theses

Combination coefficients of small ions with aerosol particles

Dixon, A. M.

How to cite:

Dixon, A. M. (1976) *Combination coefficients of small ions with aerosol particles*, Durham theses, Durham University. Available at Durham E-Theses Online: <http://etheses.dur.ac.uk/9158/>

Use policy

The full-text may be used and/or reproduced, and given to third parties in any format or medium, without prior permission or charge, for personal research or study, educational, or not-for-profit purposes provided that:

- a full bibliographic reference is made to the original source
- a [link](#) is made to the metadata record in Durham E-Theses
- the full-text is not changed in any way

The full-text must not be sold in any format or medium without the formal permission of the copyright holders.

Please consult the [full Durham E-Theses policy](#) for further details.

COMBINATION COEFFICIENTS OF SMALL IONS

WITH AEROSOL PARTICLES.

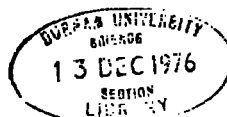
by

A. M. DIXON, B.Sc.

Submitted in candidature for the degree of M.Sc. in
the University of Durham.

The copyright of this thesis rests with the author.
No quotation from it should be published without
his prior written consent and information derived
from it should be acknowledged.

October 1976.



ABSTRACT

This work was concerned with the measurement of the variation of the combination coefficient between aerosol particles and small ions, b , with the radius of the particles. The variation of the combination coefficient between uncharged aerosol particles and small ions, η_0 , with radius was also examined.

The ion-ion recombination coefficient, α , was first evaluated from plots of small ion decay in an aerosol-free mylar vessel of volume 3.1 m^3 . Small ions were produced from corona discharge around the tip of a steel needle, set at a high voltage. 14 measurements of α were made, giving a mean experimental value of $2.39 (\pm 0.14) \times 10^{-6} \text{ cm}^3 \text{ sec}^{-1}$.

A technique was developed for simultaneous measurements of the combination coefficient b and the aerosol particle size. Particles were produced by blowing filtered air over a glowing nichrome wire. Methods of number concentration and particle size determination are described. The decay of the ions in the presence of the particles in the mylar vessel was recorded and compared with a family of theoretical ion-aerosol decay curves plotted by the computer to determine b . A total of 26 b measurements were made and the value ranged from $0.35 \times 10^{-6} \text{ cm}^3 \text{ sec}^{-1}$ to $2.24 \times 10^{-6} \text{ cm}^3 \text{ sec}^{-1}$, corresponding to radii of $0.41 \times 10^{-6} \text{ cm}$ to $4.0 \times 10^{-6} \text{ cm}$. The variation of η_0 with radius was also investigated in ten of these b measurement experiments. The value of η_0 ranged from $0.33 \times 10^{-6} \text{ cm}^3 \text{ sec}^{-1}$ to

$2.39 \times 10^{-6} \text{ cm}^3 \text{ sec}^{-1}$ for corresponding radii of $1.26 \times 10^{-6} \text{ cm}$ and $4.0 \times 10^{-6} \text{ cm}$.

Various theoretical models for combination coefficients were discussed. The b and η_0 versus radius results were compared with theoretically computed values. The discrepancy between the generally larger experimental values and theoretical values for the combination coefficients was also discussed.

*

*

*

CONTENTS.

	<u>Page.</u>
Abstract	i
Contents	iii
List of Figures	v
List of Photographs	vii
List of Tables	vii
<u>Chapter 1. General Introduction.</u>	1
1.1 Introduction.	1
1.2 Some Characteristics of Small Ions.	2
1.3 The Overall Problem.	6
<u>Chapter 2. Small Ion Generation and Measurement of Ion Mobility and Recombination Coefficient, α.</u>	10
2.1 Small Ion Production.	10
2.2 Measurement of Number Concentration and Mobility of Ions.	13
2.3 Measurement of the Recombination Coefficient, α .	16
<u>Chapter 3. The Experimental Determination of the Variation of Combination Coefficients b and η_0 with submicrometre Aerosol Particles of Radius r.</u>	20

3.1	The Mechanism of Sub-micrometre Aerosol Particle Production.	20
3.2	The Measurement of Concentration of Sub-micrometre Aerosol Particles.	22
3.3	The Measurement of Size of Sub- micrometre Aerosol Particles by the Diffusion Battery Method.	26
3.4	Ion-tube Measurements on Charged Particles.	30
3.5	Experimental Determination of b versus Radius and η_0 versus Radius.	31
<u>Chapter 4. Theoretical Calculations of Combination Coefficients.</u>		38
<u>Chapter 5. The Experimental Results of b and η_0 versus Radius compared with various Theoretical Models.</u>		49
5.1	Experimental Results.	49
5.2	Comparison with Other Experimental Results.	52
5.3	Theoretical Models for b versus Radius.	54
5.4	Comparison of η_0 versus Radius Values with Theory.	57
5.5	Conclusion.	59
References		60
Acknowledgements		65

LIST OF FIGURES.

<u>Figure.</u>		<u>Following page:</u>
2.1	Schematic Diagram of Small Ion Discharge Vessel.	10
2.2	Threshold and Critical Voltages for Small Ion Production.	on page 11
2.3	Schematic Diagram of Small Ion Tube.	13
2.4	Analysis Scheme for a Continuous Ion Spectrum.	14
2.5	Experimental Current-Potential curve for Small Ions.	14
2.6	Experimental Mobility Spectrum for Small Ions.	14
2.7	Experimental Ion-ion decay curve.	17
2.8	$\tanh^{-1}(n_p/n)$ versus Time for the Ion-ion decay curve, (2.7).	17
3.1	Schematic Diagram of the Photo-Electric Nucleus Counter.	23
3.2	The Inverting Amplifier.	24
3.3	Voltage Output For Amplifier.	24
3.4	Penetration Curves of Polydisperse Aerosols through a Parallel-walled Channel.	29
3.5	The Interpolation Curve.	29
3.6	Schematic Diagram of the Large Ion Tube.	30
3.7	Schematic Diagram of Apparatus for Measurement of b and η_0 versus radius.	32

3.8	Experimental Ion-aerosol Decay Curve.	35
3.9	Theoretical Family of Curves for Ion-aerosol Decay, $n_{\infty} = 200$.	35
4.1	Ion Trajectories (Attractive Case.)	41
4.2	Recombination Coefficient, α , as a Function of Trapping Distance.	45
4.3	Variation of δ and s_0 with Radius.	46
5.1	Variation of b with Radius.	51
5.2	Variation of η_0 with Radius.	51

LIST OF PHOTOGRAPHS.

<u>Plate No.</u>		<u>Following page:</u>
1	Measurement of Small Ion Concentration.	13
2	The Photo-electric Counter System.	25
3	Electrical Instrumentation associated with the Experimental System.	31
4	A General View of the Experimental System.	31

LIST OF TABLES.

<u>Table No.</u>		<u>Page.</u>
2.1	Results of α Determinations.	19
4.1	Values of the Enhancement Factors b_o^2 and $\langle b^2 \rangle$ for Different Radii.	44
5.1	Variation of b with Radius.	50
5.2	Variation of b and η_o with Radius.	51
5.3	Results of Flanagan (1965).	54
5.4	Theoretical Models for b versus Radius.	55
5.5	Theoretical Models for η_o versus Radius.	58

CHAPTER 1.

GENERAL INTRODUCTION.

1.1 Introduction.

Few experimental measurements exist to date of the variation of the combination coefficient between aerosol particles and small ions, b , with the particle size. The only notable series of results for simultaneous measurements of b and the particle radius have been made by Flanagan (1965), for eleven aerosol particle sizes ranging from 0.5 to 5×10^{-6} cm. Moreover, there are no known results of the variation of the combination coefficient for uncharged aerosol particles with small ions, η_0 , with the particle size. On the other hand, theoretical considerations on the variation of these combination coefficients with radius are well established, particularly by Bricard (1949, 1962), Keefe and Nolan (1961, 1962 and 1968) and Hoppel (1969, 1974). The purpose of this work is to extend the experimental study of b versus particle radius and also to determine how η_0 varies with particle radius, and to compare the experimental results with the theoretical predictions.

The following section gives a description of the properties of small ions pertinent to the proposed work, and then the overall problem of measuring the combination coefficients is outlined in the final section of this chapter.



1.2 Some Characteristics of Small Ions.

When electrons become detached from atoms or molecules in the air, they soon attach themselves to a neutral atom or molecule as they cannot exist freely at normal temperature and pressure. But under the same conditions these so formed ions also cannot remain stable and hence tend to surround themselves with neutral molecules and form into aggregates of approximately 10 to 30 molecules, becoming so called "small ions", with radii of about 10^{-6} cm. These three phases leading to ion production require only of the order of 10^{-6} seconds to take place. Wright (1936) considered the mass of these small ions to be equivalent to that of 10 to 12 water molecules, while Torreson (1939) considered the size of an ion to be about that of 4 molecules of oxygen.

The number of small ions present in the air is generally of the order of a few hundred per cm^3 ; where the concentration of positive ions (n') is found to be 20% higher than that of the negative ions (n''). In heavily polluted lower atmospheres the small ion concentration is reduced to as little as 10% or less of its normal value, and the same characteristic is shown in clouds.

One of the main physical characteristics of small ions in the atmosphere (with given temperature and pressure) is their mobility, which describes the speed the ion has in the given environment under the action of an electric field of 1 volt per cm. Under normal conditions the measured positive ion mobility (k') is

1.4cm²/V sec and the corresponding negative ion mobility (k'') is 1.9cm²/V sec. The mobility varies with pressure (p) and temperature (T) as follows:

$$k(p, t) = k_0(p_0, t_0) \frac{p_0}{p} \cdot \frac{T}{T_0} \quad (1.1)$$

where p₀ and T₀ are the N.T.P. values. The conductivity, Λ, of the air arises as a direct consequence of the concentration of small ions and of their mobility, and is given by:

$$\Lambda = (k'n' + k''n'')e \quad (1.2)$$

where e represents the elementary charge.

Another important characteristic of small ions is their diffusion coefficient. Let $\frac{dn}{dz}$ be the concentration gradient of positively or negatively charged ions in a direction OZ at a given point O. The flux of ions traversing a 1 cm² area centred on O and normal to OZ is equal to $-D \frac{dn}{dz}$ where D is the diffusion coefficient of the ions, with units of cm²sec⁻¹. The mobility and diffusion coefficients are connected by the Einstein relation:

$$\frac{k}{D} = \frac{e}{k_B T} \approx \frac{1}{40} \quad (\text{N.T.P.}) \quad (1.3)$$

If one neglects the effect of the electric field produced by the small ion (sufficiently strong to polarise neighbouring molecules) one can apply results of kinetic theory and obtain an expression of the mobility in terms of the masses m of the small ions and M of the

air molecules introducing the mean free path, λ , and mean thermal velocity, \bar{v} , of the air molecules, as in the Langevin expression:

$$k = 0.75 \frac{e\lambda}{M\bar{v}} \sqrt{\frac{m+M}{m}} \quad (1.5)$$

which is probably the most satisfactory expression for the mobility of small ions. This expression will be used in the analysis of the experimental results to deduce a value of the mean free path, λ , for a selected value of the ionic mass, m , using the expression $\bar{v} = \sqrt{8kT/M}$ to obtain the mean thermal velocity of the air molecules.

'Rival' expressions given by Kennard (1938) for the mobility and diffusion coefficient of small ions:

$$k = \frac{3}{8} \sqrt{\pi} \lambda e \left(\frac{m+M}{mM} \frac{1}{k_B T} \right)^{1/2} \quad (1.6)$$

$$D = \frac{3}{8} \sqrt{\pi} \lambda \left(\frac{m+M}{mM} k_B T \right)^{1/2} \quad (1.7)$$

have been used by Bricard to deduce a value for λ . He assumed $M = m$, and assumed $k = 1.4 \text{ cm}^2/\text{V sec}$ and found $\lambda = 1.3 \times 10^{-6} \text{ cm}$. This is markedly different from the value deduced from viscosity measurements, for air molecules: $\lambda = 6.4 \times 10^{-6} \text{ cm}$ (at N.T.P.). One must stress here that the assumption $M = m$ cannot apply if we accept to any degree the idea of the small ion cluster comprising of several molecules. Values obtained by other authors will be discussed in Chapter 5.

In the absence of aerosol particles, the rate at which the

number of small ions varies with time may be written as:

$$\frac{dn}{dt} = q - \alpha n^2 \quad (n' = n'' = n) \quad (1.8)$$

where n is the number of small ion pairs per cm^3 , q the number of ion pairs produced per cm^3 per second by the ionizing agency, and the quantity α is defined as the recombination coefficient of small ions, having the dimensions of $\text{cm}^3\text{sec}^{-1}$. The recombination coefficient, α , indicates the probability of a collision occurring per second when the unit volume contains one positive and one negative ion.

If the number of ions destroyed per unit time by recombination is equal to the number produced per second by the source of ions, then ionization equilibrium has been attained (assuming n' and n'' are equal).

Hence:

$$\frac{dn}{dt} = q - \alpha n^2 = 0 ; \quad q = \alpha n_{\infty}^2 \quad \text{or:} \quad n_{\infty} = \sqrt{\frac{q}{\alpha}} \quad (1.9)$$

where n_{∞} is the equilibrium ion concentration. Integration of the above equation yields:

$$\tanh^{-1}\left(\frac{n_{\infty}}{n}\right) = n_{\infty} \alpha t + \tanh^{-1}\left(\frac{n_{\infty}}{n_i}\right) \quad (\text{if } n_i > n_{\infty}) \quad (1.10)$$

n_i and n_{∞} representing the initial and final concentrations respectively. If $n \gg n_{\infty}$ then $\tanh^{-1}(n_{\infty}/n)$ tends to n_{∞}/n and the above equation simplifies to become:

$$\frac{1}{n} - \frac{1}{n_i} = \alpha t \quad (1.11)$$

a result which can also be obtained by integration of the equation $dn/dt = \alpha n^2$. This result is widely used experimentally in determining α , by setting $q = 0$ at a given instant in time (t). In this work the

equilibrium ion concentration n_{∞} was always strictly comparable with n in ion recombination experiments, and equation (1.10) was used to determine the value of α .

1.3 The Overall Problem.

The rate of change of small ions in the atmosphere must include terms (not required hitherto) allowing for the effect of the atmospheric aerosol content and the fair weather field. In general, we can write:

$$\frac{dn}{dt} = q - \alpha n^2 - n\beta_1 - n\beta_2 - n [\text{field factor}] \quad (1.12)$$

where β_1 and β_2 represent the dissipation constant due to aerosol particles and 'precipitation' particles (for example, cloud droplets) respectively. The field factor has been evaluated by Gunn (1954) and accounts for the loss of ions via conduction to cloud droplets. This effect only begins to dominate over diffusion losses in field values of greater than 0.1 e.s.u.. The field factor can normally be neglected in considering ionic equilibrium since the fair weather field is only of the order of $1/300$ e.s.u.. Experiments are carried out in the absence of precipitation particles and so the β_2 term can be ignored for the experimental conditions. So in the case of small ion equilibrium we are left with the condition:

$$\frac{dn}{dt} = 0 = q - \alpha n^2 - n\beta_1 = q - \alpha n^2 - \eta_0 n N_0 - \eta n N \quad (1.13)$$

or:

$$q = \alpha n^2 + bZn \quad (1.14)$$

where $b = \frac{(\eta_0 N_0 + \eta N)}{Z}$ and $Z = N_0 + 2N$, the total concentration of

particles. N_0 is the number of uncharged particles per cm^3 ; N is the number of large ions per cm^3 ; η_0 is the combination coefficient for small ions and uncharged aerosol particles; η is the combination coefficient for small ions and large ions of opposite sign. The effects of multiple charged nuclei have not been included here: for atmospheric nuclei of radius $\leq 6 \times 10^{-6}$ cm it is a fairly good approximation to consider that only neutral and singly charged nuclei are present. From above:

$$\beta_1 = \frac{q - \alpha n_\infty^2}{n_\infty} \quad (1.15)$$

A solution of the equation $\frac{dn}{dt} = q - \alpha n^2 - \beta_1 n$ can now be obtained using relation (1.15) for β_1 and denoting the concentration of small ions at $t = 0$ by n_0 :

$$\frac{n(t) + q/\alpha n_\infty}{n(t) - n_\infty} = \exp(A\alpha t + k') \quad (1.16)$$

where:

$$A = n_\infty + q/\alpha n_\infty \quad ; \quad k' = \ln \left(\frac{n_0 + q/\alpha n_\infty}{n_0 - n_\infty} \right)$$

The equilibrium ion concentration (n_∞) is clearly dependent upon (i) the effective recombination coefficient b between small ions and aerosol particles and (ii) the particle concentration Z and (iii) the ion generation rate q .

A similar equation to (1.13) can be written for large ions:

$$\frac{dN}{dt} = \eta_0 n N_0 - \eta n N \quad (1.17) \text{ (Multiple charging ignored)}$$

Similarly, if large ion equilibrium exists, $\frac{dN}{dt} = 0$ and:

$$\eta_0 N_0 = \eta N \quad (1.18)$$

Putting $\eta/\eta_0 = l$ and $Z = N_0 + 2N$ one may write in the case of large ion equilibrium:

$$b = \frac{2\eta_0 l}{l+2} \quad (1.19)$$

For non-equilibrium the factor f is introduced as a measure of the departure from equilibrium, such that $N_0/N = f$, (where $f = 1$ for equilibrium). Then we have:

$$\frac{b}{\eta_0} = \frac{l(1+f)}{fl+2} \quad (1.20)$$

As stated in the introduction, the purpose of the work described in the following chapters is firstly to obtain a set of values of the combination coefficient b for different values of radii, including the range commonly encountered in the atmosphere ($a \sim 1$ to 5×10^{-6} cm), and secondly to procure measurements of η_0 versus radius. The latter section of the experiment is accomplished by simultaneous measurements of b , Z/N_0 , $(Z/N_0)_\infty$ and radius. η_0 is then evaluated through the use of equation (1.20). Experiments involve measurements of size and concentration of aerosol particles produced by a glowing nichrome wire, and the measurement of the decay of small ions in the presence of the aerosol particles in a mylar reservoir, of volume 3.1 m^3 . Decay curves for the small ions obtained for a particular size and concentration of aerosol particles were compared with theoretical decay curves plotted from relation (1.16) using a 'family of curves' technique to evaluate β (and hence b). Values of η_0 could then be

determined by application of equation (1.20), using the measured values of (Z/N_0) , $(Z/N_0)_\infty$ to obtain f and l .

It was necessary to find a value of α for the small ions measured in the enclosed storage vessel, in order that all the parameters of equation (1.16) could be associated with conditions in the storage vessel. The following chapter gives an account of the method employed for measuring α and displays the results obtained over the period during which ion-aerosol combination coefficient measurements were performed. A full survey of the experimental procedures undertaken for b and η_0 measurements is given in chapter 3. Chapter 4 discusses various theoretical models proposed for predicting the relationships of b and η_0 with radius, giving particular attention to the importance of image capture and three-body trapping in calculating the ion-aerosol attachment coefficients for aerosol particles of small radii. The final chapter gives an analysis of the results obtained from this work and discusses them in the light of theoretical considerations and previous experimental measurements.

*

*

*

CHAPTER 2.

SMALL ION GENERATION AND MEASUREMENTS OF ION MOBILITY AND RECOMBINATION COEFFICIENT, α .

2.1 Small Ion Production.

The small ions for this work were produced by corona discharge at the point of a steel needle. The design of the ion source apparatus was based on the small discharge vessel which Nolan and O'Toole (1959) used for the production of condensation and small ions, but was modified to suit the requirements of this experiment.

The discharge vessel comprised of a brass cylinder 11cm long and 6.3cm in diameter, shown in figure (2.1). The needle used was an ordinary steel sewing needle, which was set at a positive potential from an E.H.T. supply; the brass ring and the whole of the brass cylinder were earthed. The ions produced by corona discharge around the needle were dissipated by a filtered air flow, and the ions were collected in a 3.1 m^3 rectangular mylar vessel, where all experiments were carried out.

The positive potential applied to the needle was carefully chosen such that it was below the critical voltage for condensation nucleus production, but above the critical voltage of ion production. Nolan and Kuffel (1957) have examined the critical voltages required for nucleus production and for small ion production by point discharge, and have shown that in the latter case the critical voltage was lower, for a particular needle. They also found the predictable

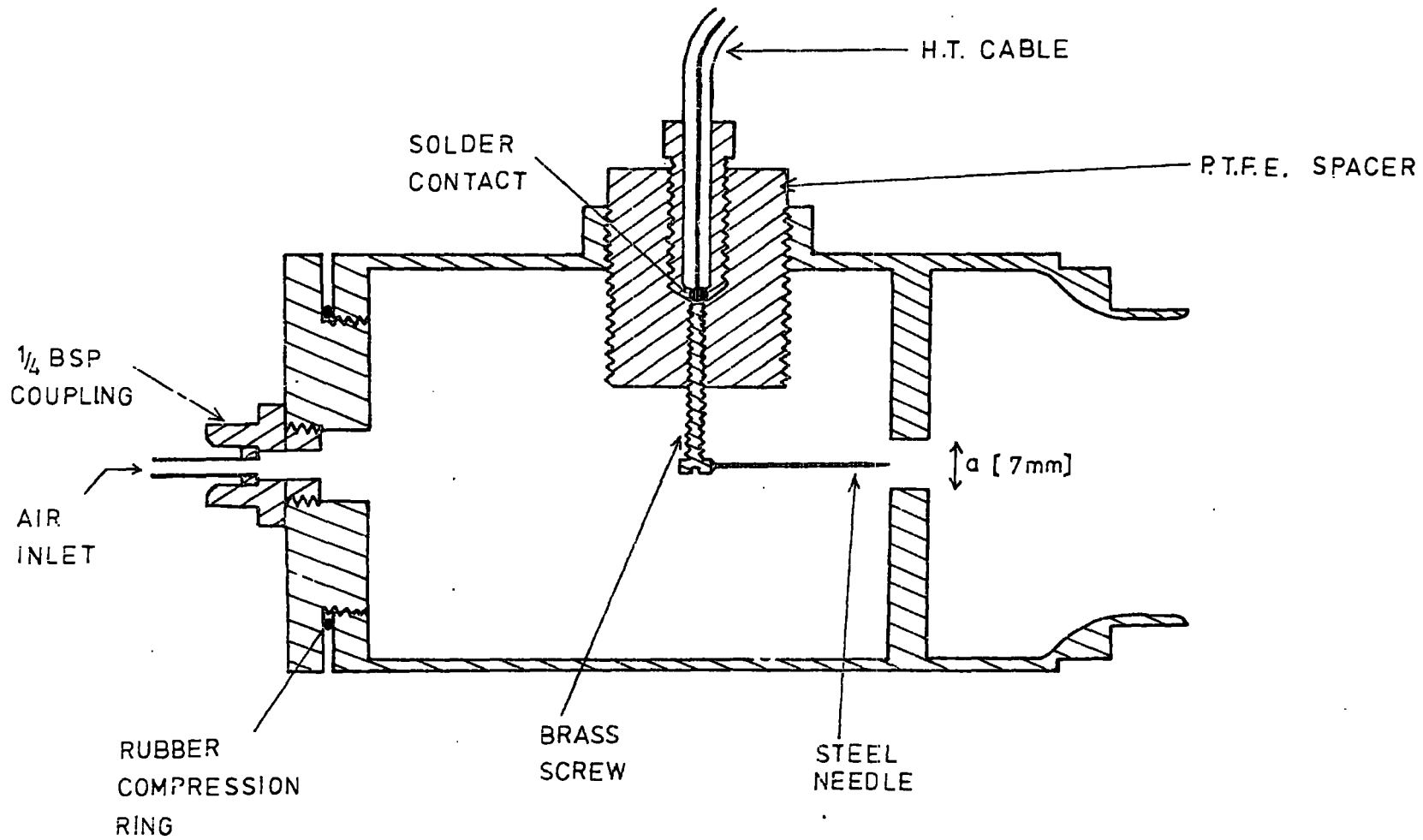
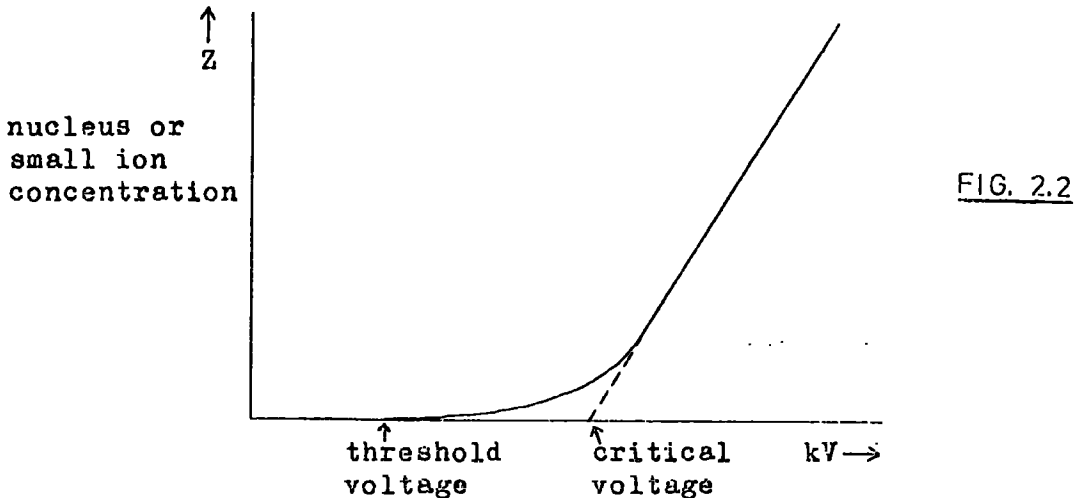


FIG. 2.1 Schematic Diagram of Small Ion Discharge Vessel.

[To Scale.]

result that the critical voltage depended on the sharpness of the needles.

The actual threshold voltage is lower than this, as illustrated in figure 2.2 below:



The critical voltage is thus the voltage at which Z begins to increase rapidly. More recent work by Nolan and O'Toole (1959) indicates that the threshold voltage for small ion and nucleus production are the same. This infers that although the value of the potential was adjusted to be below the critical voltage for nucleus production for all experiments, there may have been a very low concentration of nuclei actually produced. However, the Nolan-Pollak photo-electric counting system employed here for measuring nuclei concentrations (see chapter 3) registered less than 100 particles per cm^3 with 16cm Hg overpressure for samples of ions taken from the mylar vessel. This low concentration revealed that there was no nett increase in nuclei in the enclosed space due to the ion production mechanism, taking into account the efficiency of the mylar vessel in excluding all aerosols from the laboratory environment. It may be noted that concentration measurements were not only taken just after production

of ions, when condensation nuclei if produced are likely to be very small; they were also taken after being stored sufficiently long to allow coagulation out of the unobservable size region of the photo-electric counter, but no significant increase in concentration was observed.

Corona point discharge is caused by a non-uniform field of considerable strength in the region surrounding the point. Such a field is also a very efficient collector of the ions, so that a high velocity flow rate is required to free the ions from the electric field in order that a high concentration of small ions can emanate from the ion source. Hence the relatively inefficient producer of 'free' ions used by Nolan and O'Toole (1959) has been modified to suit the purpose of this work by the introduction of the narrow slit 'a', shown in figure 2.1. The width of 'a' was chosen for a suitable yield of small ions, with the potential in the range of 2 to 3 kV, and with a flow rate of 40 litres per minute. The needle was positioned such that its tip was concentric with the slit, as in figure 2.1. Such modifications to the apparatus follow the principles of the sonic jet small ion generator described by Whitby and McFarland (1961), but the velocity across the needle point here was only of the order of $\frac{1}{20}$ the velocity of sound. Nevertheless a concentration of $\sim 10^7$ ions per cm^3 was usually recorded at a distance of about 15cm from the source, which proved an adequate initial flux of ions.

A multi-needle ion source was also constructed (using the same principles as the single needle source) in case higher ionic concentrations were required, but this was found to be superfluous in subsequent experiments.

2.2 Measurements of Number Concentration and Mobility of Ions.

Ionic concentrations were measured using a cylindrical aspiration capacitor (small ion tube), shown in plate 1 and schematically in figure 2.3. Air from the mylar vessel was drawn through the cylindrical electrode A at a flow rate of 50 litres per minute. This electrode is shielded from stray electric fields by a larger earthed concentric cylinder and insulated from it by P.T.F.E. rings. A positive polarising voltage is applied to electrode A which causes ions of the same sign to be deflected towards the central rod B, insulated from the other two electrodes by the P.T.F.E. spacer, C. A solid state Keithley electrometer (model 602) connected to the central electrode B records the resulting ion current. The air was drawn through the ion tube by means of an electric pump and the flow was monitored by a 0 to 100 litre/min rotameter.

If V is the potential difference between the cylinder A and the central electrode B, then the electric intensity, E , at a point r from the central axis is:

$$E = \frac{V}{r \log_e a/b} \quad (2.1)$$

where a and b are defined in figure 2.3. Ions of mobility ω move a radial distance $dr = \omega E dt$ in time dt . Consider an ion starting at the outer cylinder A and moving inwards toward the central electrode B; the time taken to traverse the radial distance dr is:

$$dt = \frac{dr}{\omega E} = \frac{r \log_e a/b dr}{\omega V} \quad (2.2)$$

The total time taken to get from the outer cylinder A to the central



PLATE 1. Measurement of Small Ion Concentration.

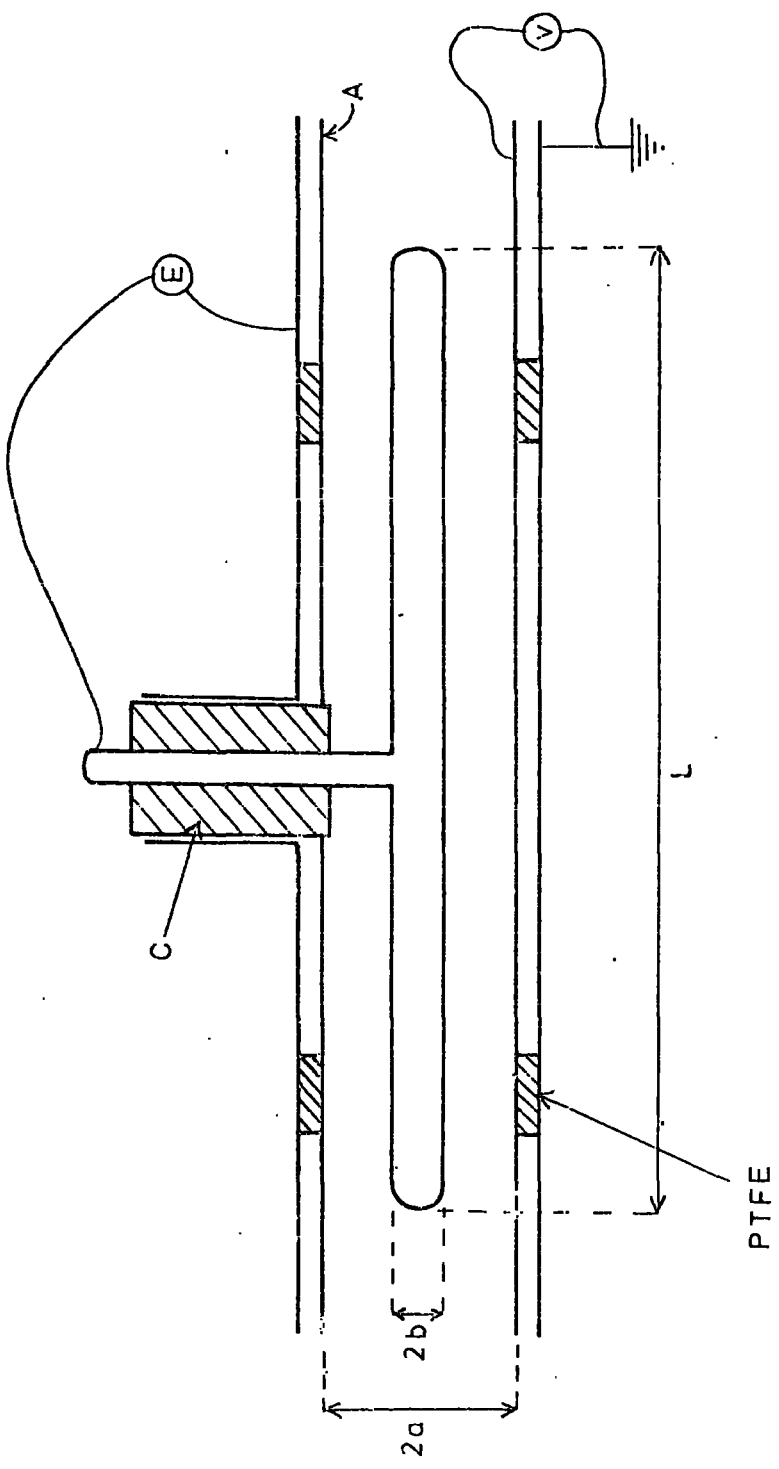


FIG. 2.3

electrode B is:

$$t = \frac{(a^2 - b^2)}{2} \cdot \frac{\log_e a/b}{\omega V} \quad (2.3)$$

During this time air will have moved a distance ut along the cylinder, where u is the velocity of the air flow. If this distance is less than L , then all inward moving ions will be collected. Hence all ions are collected if $u < L/t$ or:

$$u < \frac{2 \omega V L}{(a^2 - b^2) \log_e a/b} \quad (2.4)$$

So we can define a critical mobility ω_c , and for a particular V and volume flow rate $Q (= u\pi(a^2 - b^2))$ all ions with mobility ω_c will be captured, where ω_c is given by the relation:

$$\omega_c = \frac{Q \ln a/b}{2\pi V_c L} \quad (2.5)$$

By varying the voltage, V a mobility spectrum for the small ions can be obtained experimentally using the method described by Israel (1971). The concentration of small ions is plotted as a function of the applied voltage, as in figure 2.4. Israel shows that the intercept $OP (i - V \frac{di}{dV})$ on the ordinate axis gives directly the total number of ions with mobility $\omega \geq \omega_c$, where ω_c is calculated from the corresponding V values (equation 2.5). Hence $OP - OP'$ gives the number of small ions trapped in the voltage range V_c' to V_c (corresponding to the mobility range ω_c to ω_c').

Experimental results of small ion mobility using this technique are shown in figures 2.5 and 2.6. Small ions were introduced into the mylar vessel for 3 minutes, and then the vessel was 'closed off' for a period of time sufficiently long for the small ions to attain a state

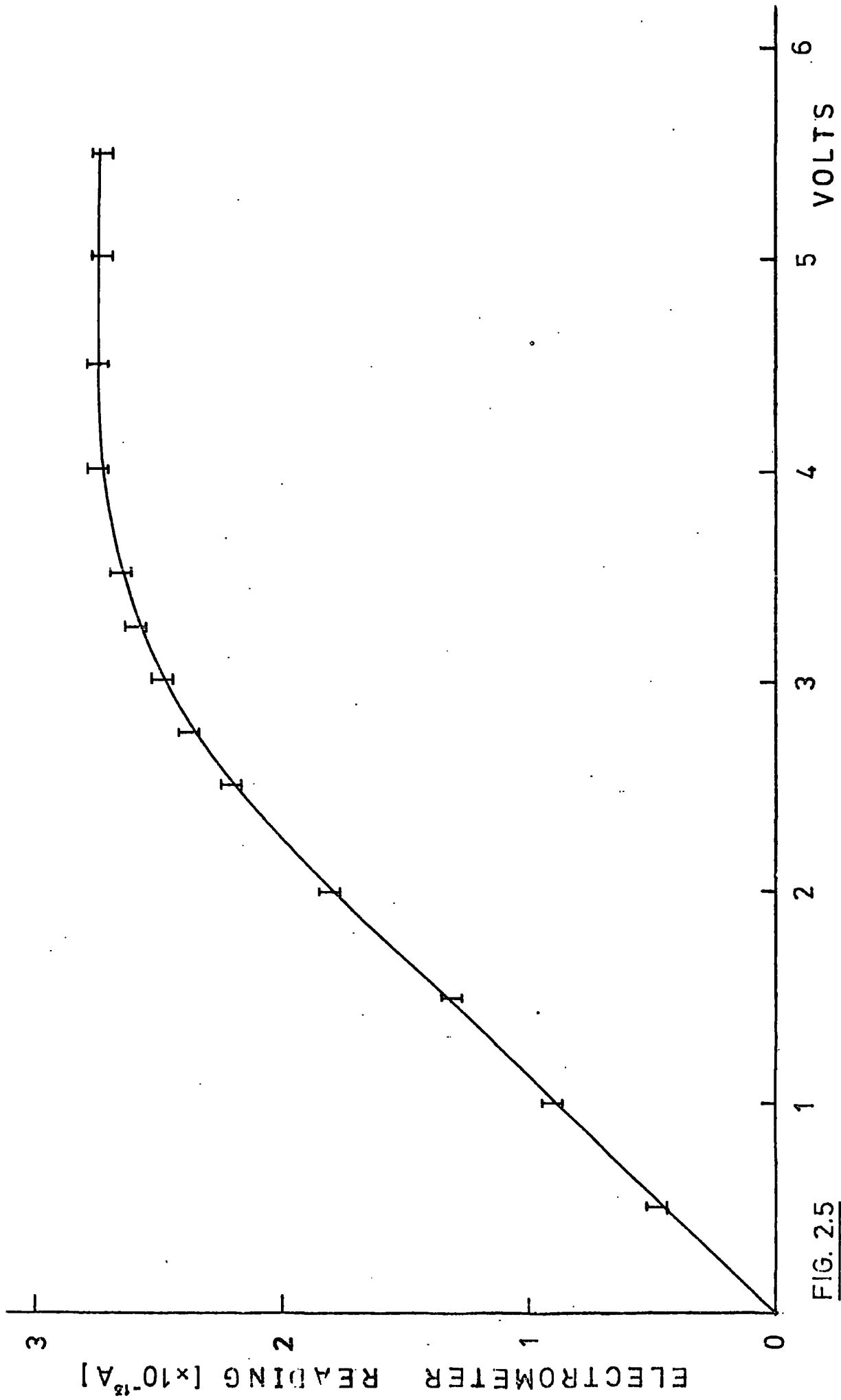


FIG. 2.5

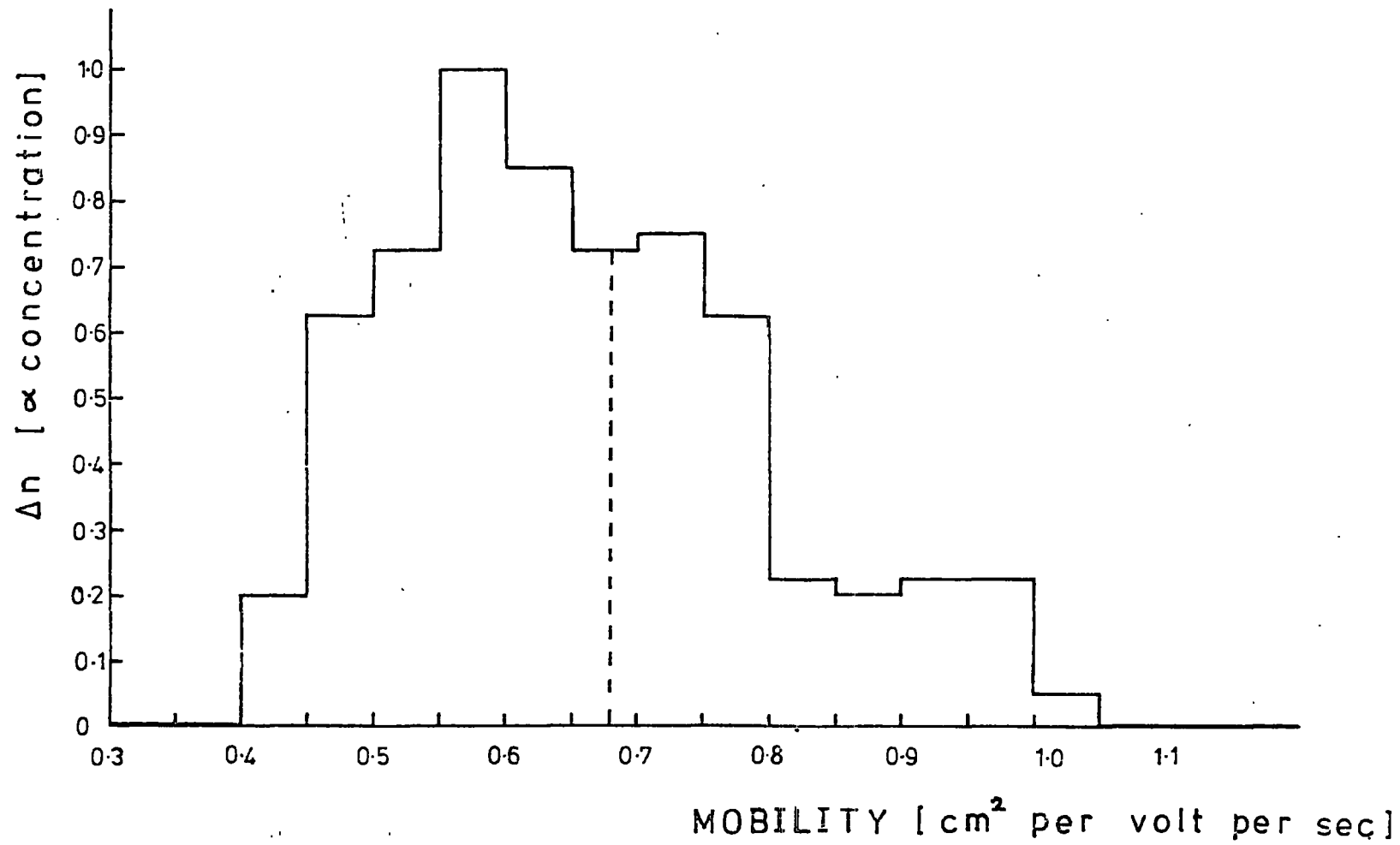


FIG. 2.6

of equilibrium (about 10 minutes). The resulting ion concentration (~ 2000 per cm^3) was sampled by the ion tube at 30 litres/min. for voltages ranging from 0 to 6 volts. It was necessary to calibrate the electrometer before commencing the experiment so that it would display a reading of zero with zero volts across the co-cylindrical condenser. Without this adjustment a small negative ionic concentration was recorded for zero volts.

In the experiment the electrometer was connected to an ultra-violet recorder so that a continuous record of current was recorded for each voltage chosen. Each point on figure (2.5) corresponds to an electrometer reading averaged over 90 seconds, after allowing for the logarithmic rise due to the response time of the electrometer. Tangents at chosen values of V enabled the mobility spectrum in figure 2.6 to be determined. Values of the parameters in equation 2.5 were: $a = 1.742\text{cm}$, $b = 0.635\text{cm}$, $L = 37.3\text{cm}$, $Q = 30$ litres/min. The mean mobility is estimated to be $0.68\text{cm}^2\text{V}^{-1}\text{sec}^{-1}$.

An experiment was devised to estimate the number of small ions produced per second at the slit of the ion source. This involved having the ion aspirator flush with the ion source; the ion source had been designed to fit snugly into the outer cylinder of the ion aspirator. With 20V across the ion tube, and a flow rate of 50 litres per minute across the needle, a time-averaged value of $1.1 \times 10^{-9}\text{A}$ was recorded on the electrometer. This value was obtained by analysis of the continual trace on the U/V recorder output: fluctuations in the output only amounted to a maximum of 5% of the magnitude of the reading. This corresponds to a concentration of 8.3×10^7 ions per cm^3 . The initial absolute value of the small ion concentration is

difficult to determine, since the decay of ions at such high concentrations is very rapid, as found by Whitby and McFarland (1961). However with a flow rate of 50 litres/min. through the narrow orifice (7mm diameter) the time taken to reach the electrodes is only of the order of a few hundredths of a second. Hence 10^8 ions per cm^3 as an order of magnitude would appear to be a good estimate for the ionisation rate 'q' of the source.

2.3 Measurement of the Recombination Coefficient, α .

Determination of the recombination coefficient, α was made using the same arrangement as for the mobility measurement. Decay of small ions in a closed space with no source has been examined by Whitby and McFarland (1961), and they have shown that the concentration of ions left after time, t is independent of the size and shape of the closed space, and hence that the decay rate of the cloud of ions is only dependent on the properties of the cloud itself. The diffusion of ions to the boundary of the vessel should however be considered as an agent in the decay of the ions; this has been examined by Flanagan (1965). He modified the equation for small ion decay in the presence of aerosol particles by the inclusion of a diffusion loss term, $D\nabla^2 n$, in the equation:

$$\frac{\partial n}{\partial t} = D\nabla^2 n + q - bZn - \alpha n^2 \quad (2.6)$$

with the boundary condition that $n = 0$ at the walls of the vessel. For equilibrium conditions in a spherical vessel this equation has the solution:

$$n = n_e \left(1 - \frac{a \sinh kr}{r \sinh ka} \right) \quad (2.7)$$

where $k^2 = bZ/D$ and $n_e = q/bZ$. For a balloon of radius 60cm (half the width of the rectangular mylar vessel), and with $k = 0.5\text{cm}^{-1}$, the diffusion loss is negligible apart from within the region about 10cm from the balloon wall. The diffusion loss for air free of aerosol particles was estimated from equation 2.7 by putting $k^2 = \alpha n/D$. This effectively calculates the loss of positive ions by diffusion and recombination, and estimates showed that the diffusion loss would again be negligible within about 10cm from the walls of the vessel. In all experiments in this work the ion-tube was projected about 30cm inside the mylar vessel, so that the diffusion loss was unlikely to affect the results.

The same method was applied for every α determination. Initially the mylar balloon was almost completely filled with filtered air: then the small ions were introduced into the vessel via a filtered air flow of 40 litres per minute, until the initial concentration was of the order of 10,000 ions, when the air flow to the needle was switched off. The particle decay was monitored on the U/V recorder with the electrometer set on the appropriate scale for current measurement. In each experiment a trace of the decay was obtained on U/V paper starting from an initial concentration of around 4000 particles (where the time, t , was arbitrarily set to zero) to the equilibrium value of generally around 2000 particles. Figure 2.7 is a replica of the decay recorded in the fifth experiment to measure α . This curve was analysed to give a value for α through the use of equation (1.10) from chapter 1. A value of the equilibrium concentration

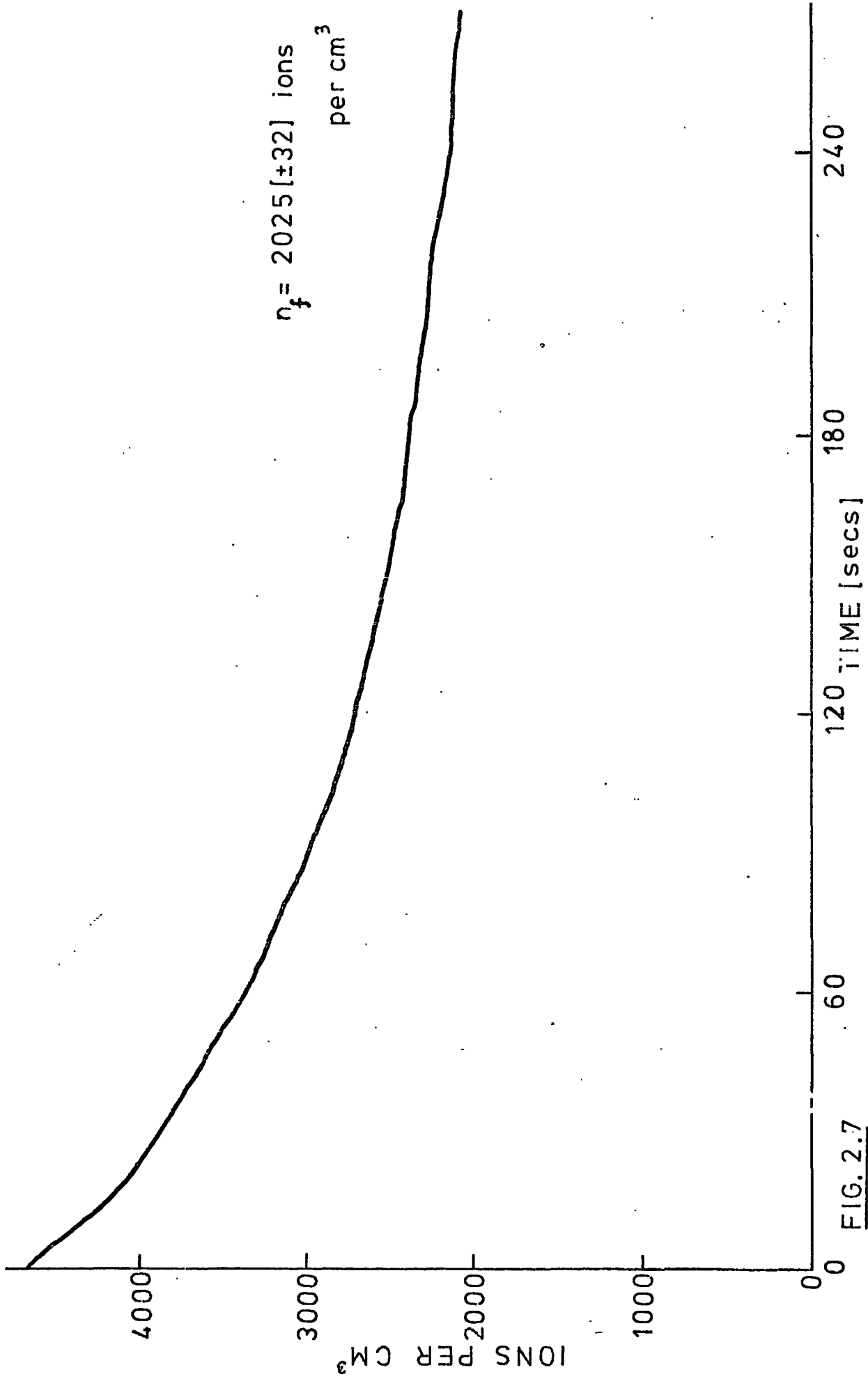


FIG. 2.7

$n_f = 2025[\pm 32]$ ions per cm^3

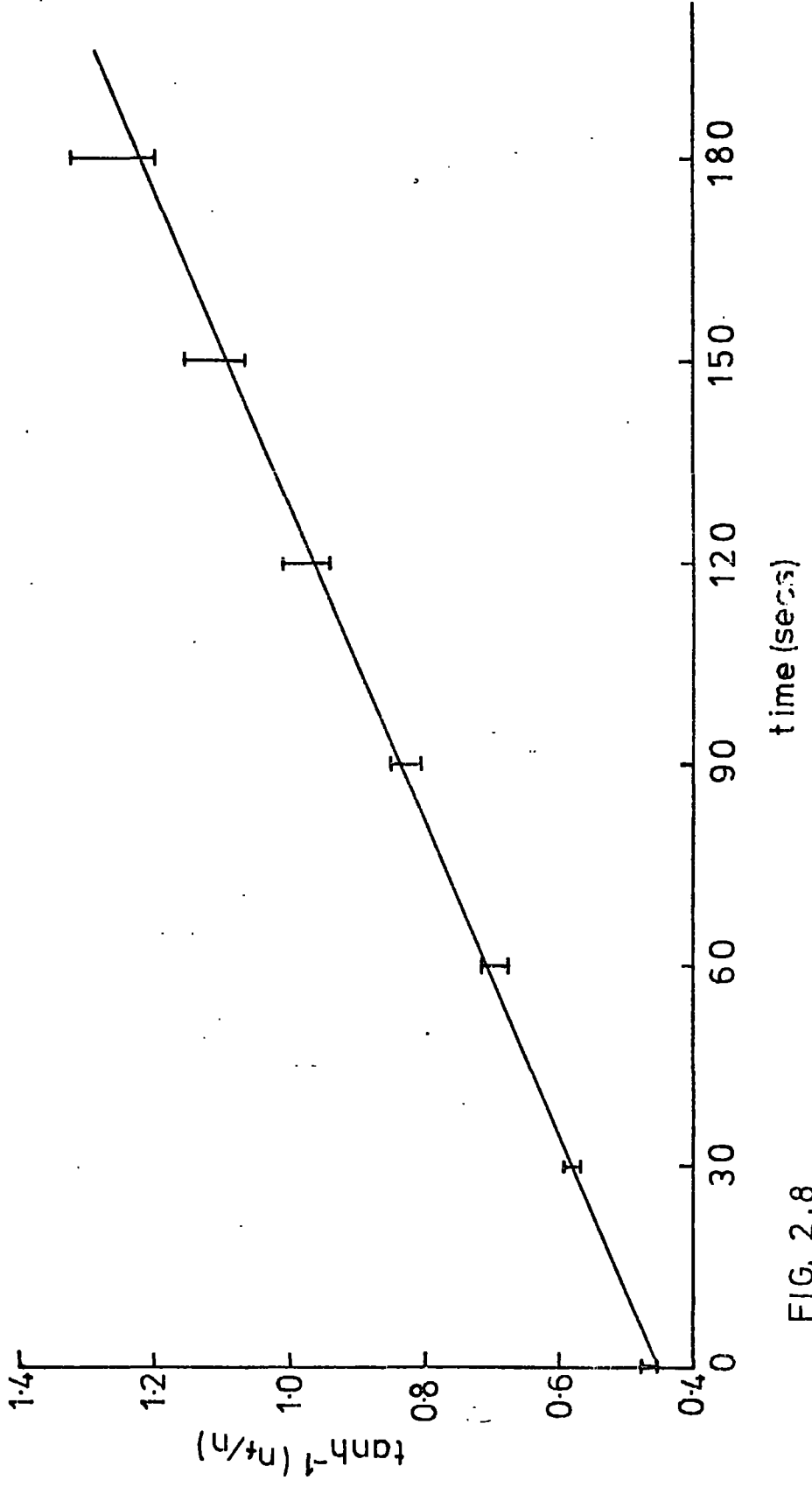


FIG. 2.8

n_{∞} was taken after leaving the apparatus running for 10 minutes. Samples of the concentration along the decay curve were taken every 30 seconds for 3 minutes starting from the initial concentration chosen, at $t = 0$. Then values of $\tanh^{-1}(n_{\infty}/n)$ were plotted versus time, and from the slope of the graph ($= n_{\infty}\alpha$), the value of α could be determined. Figure 2.8 shows the result of this procedure for the decay curve given. The error bars on the graph were evaluated on the assumption that all concentration readings from the U/V paper were accurate to ± 0.1 cm (or ± 32 ions). This entails that as the value of n_f/n gets larger, the error increases. The \tanh^{-1} function tends toward infinity as n_f/n approaches unity and it magnifies the error as the concentration approaches the equilibrium value. The best straight line was fitted through the points and a value for α calculated from its slope. The error in α was estimated by drawing lines of the maximum and minimum realistic slope through the error bars.

Two sets of α measurements were carried out, one preliminary to the first set of b measurements, the second after the second set of b (and η_0) measurements. The results for the 14 α determinations carried out are tabulated on the following page. The weighted mean of all the results gives a value of $2.39 (\pm 0.14) \times 10^{-6}$ for α . This is noticeably different from the accepted value of 1.6×10^{-6} for the atmosphere (Chalmers, 1967), but comparable with the value of 2.5×10^{-6} obtained by Whitby and McFarland, where investigations were carried out under similar conditions of high concentration of ions. The value of $\alpha = 2.39 \times 10^{-6}$ was used in the experimental determinations of b , for combination between ions and particles.

Table 2.1 Results of α Determinations.

Set and Run No.	n_f (ions. cm^{-3})	α ($10^{-6} \text{cm}^3 \text{sec}^{-1}$)
(1). 1	1393 (± 32)	2.52 (± 0.10)
2	1961 "	2.65 (± 0.27)
3	2379 "	2.41 (± 0.21)
4	1929 "	2.13 (± 0.17)
5	2025 "	2.22 (± 0.12)
6	1993 "	2.80 (± 0.10)
(2). 7	1639 "	3.03 (± 0.30)
8	1639 "	2.84 (± 0.32)
9	1543 "	1.99 (± 0.19)
10	2025 "	2.11 (± 0.16)
11	1704 "	2.33 (± 0.17)
12	1639 "	1.96 (± 0.11)
13	1993 "	2.51 (± 0.14)
14	1915 "	2.54 (± 0.28)

*

*

*

CHAPTER 3.

THE EXPERIMENTAL DETERMINATION OF THE VARIATION OF COMBINATION COEFFICIENTS b AND η_p WITH SUB- MICROMETRE AEROSOL PARTICLES OF RADIUS r .

3.1 The Mechanism of Sub-micrometre Aerosol Particle Production.

Particles were produced by blowing filtered air over a glowing nichrome wire, which was enclosed in a cylindrical container, 18cm in diameter. This cylinder had conical ends, so that the airflow through the inside was as stream-lined as possible. A 50cm length of 24 s.w.g. (0.0559cm) nichrome wire was used, which was coiled around the shank of a Gallenkamp immersion thermocouple (type PX-096), consisting of a platinum-iridium junction surrounded by an aluminous porcelain sheath of 1 cm external diameter. The thermocouple was connected to the appropriate pyrometer (type PX-075). The ends of the nichrome wire were connected to a power supply, capable of delivering a current of 10 A with a potential difference of 18 V across the specimen.

The production of condensation nuclei by a heated wire was first observed by Coulier in 1875. Since then, many investigators researching the behaviour of aerosols have used these nuclei as a source of sub-micrometre particles. Megaw and Wiffen (1964), using neutron activation techniques, have demonstrated that the nuclei produced by heated wires contain atoms of the constituent of the wire; for nichrome wire the nuclei consist mainly of chromium.

O'Connor and Roddy (1966) distinguish between 'transient' and 'permanent' nucleus production from heated wires. The transient type of nuclei are due to surface contamination, and are produced at lower temperatures than the threshold temperature for permanent nucleus production. All the 'layers' of contamination nuclei will be driven off the wire if the current is increased enough for the wire to glow brightly. Each wire used was subjected to a current of 8 A for an hour, before experimental investigations into the aerosol particle size and concentration were made, to remove all the transient type nuclei from the environment under study. The wire is then said to be 'fatigued' and only capable of permanent nucleus production. O'Connor and Roddy checked that the production was indeed permanent by keeping a 13cm length (34 s.w.g. diameter) wire heated to about 900°C continuously for seven days while passing filtered air over it at a flow rate of 3 litres per minute. The value of Z varied diurnally by almost 40% of the average value of 266000, but did not show a tendency to decrease with time. These fluctuations may have been due to changes in room temperature.

Small nuclei are produced in this way and subsequently grow by coagulation. Previous work by Nolan and Kennan (1949) and O'Connor and Roddy (1966) indicate that the minimum size measureable using a diffusion method is about 1×10^{-7} cm. Low concentrations and high flow rates are required for the minimum size, to suppress coagulation before the particles are measured for size and concentration. In this work, however, a range of sizes is required, so the facility of storage is necessary to allow particles to

coagulate, and the mylar vessel was used for this purpose. The initial concentration of nuclei from the wire was varied by means of the current through the wire. In experiments, currents ranged from 6.8 A to 8.5 A (with corresponding temperatures of 570°C and 700°C). A high flow rate of 40 litres per minute was passed over the wire to decrease the degree of heterogeneity of the nuclei, and to ensure that a large concentration of nuclei could be transported per second into the mylar vessel (without large diffusion loss to the inter-connecting $\frac{1}{4}$ " pneuflow tubing). With this arrangement, a concentration of upto 200,000 particles per cm^3 could be recorded from the mylar vessel after 4 minutes with a high current through the wire, and conversely a concentration of around 30,000 particles per cm^3 after the same time had elapsed with a low current. With a suitable time for storage a size range from 0.5 to 5×10^{-6} cm was obtained for experimental investigations.

3.2 The Measurement of Concentration of Sub-micrometre Aerosol Particles.

These condensation nuclei are so minute that they cannot be seen with any optical microscope directly, but their presence can be shown by conversion into droplets, which magnifies their size several times. The number of nuclei can then be counted assuming that each droplet is formed from only one nucleus. The formation of droplets around the condensation nuclei in a fixed volume of air saturated with water vapour can be achieved by creating a

selected supersaturation through the increase of the pressure in the vessel. The sudden expansion of the enclosed volume of air occurs adiabatically with a resultant degree of supersaturation in the vessel.

Concentration measurements for this work were made with a photo-electric condensation nucleus counter, where the concentration is obtained by measuring the extinction of a light beam passing through the fog formed by the expansion using a photocell. This is known as a relative condensation nucleus counter, for the droplets are not counted directly. The one used was a standard direct beam photo-electric counter, following the specifications of Nolan and Pollak (1946), and shown schematically in figure 3.1.

The vertical brass tube shown is 60cm long and 3.85cm in diameter, and is lined with moist blotting paper, creating a saturated atmosphere inside. The ends of the tube are sealed by glass plates and rubber compression rings. The inner sides of the glass plates are coated with a plastic demist film which prevents quantities of water condensing out on the surfaces. A lamp system is fitted at the top producing a parallel beam of light which strikes a photocell at the bottom. The photocell current (I_0) is set at a convenient value by adjusting the stable power supply to the lamp. Air samples under investigation for nuclei are drawn through the fog-tube for a time sufficiently long to ensure that the previous content is completely removed and the fog-tube is filled with the air under investigation. Filtered air is pumped

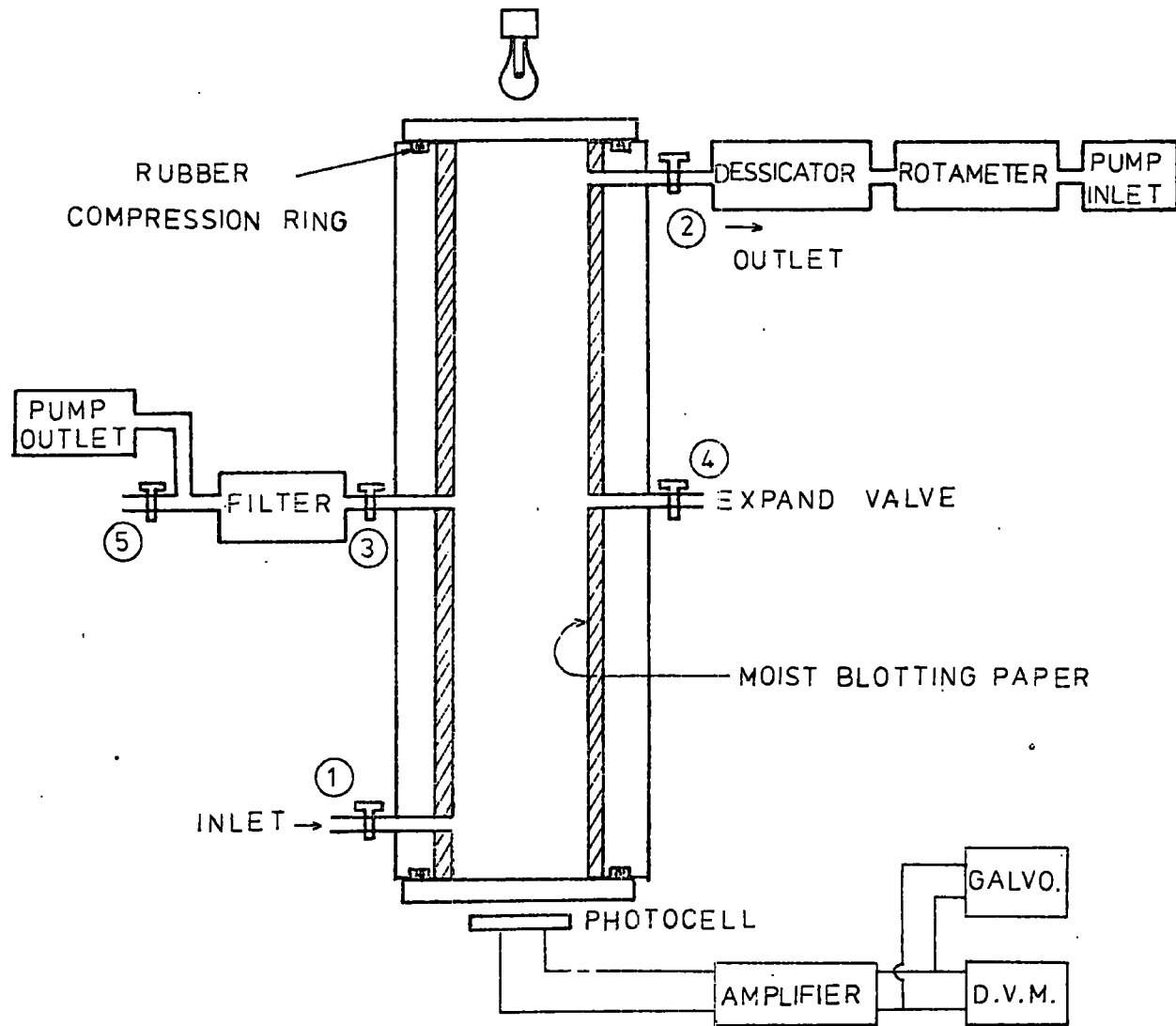


FIG. 3.1

into the counter until an overpressure of 160mm Hg is reached. This is maintained for sufficient time to allow the air to become saturated with water vapour and lose its heat of compression. The pressure is then released and the photocurrent (I_0) is measured. The sudden expansion cools the moist air and the resulting fog causes a drop in the photocurrent to a new value (I).

Nolan and Pollak (1946) have determined experimentally the relationship between extinction, $E = (I_0 - I)/I_0$ and the concentration, Z and tabulated their results for various overpressures. The absolute values of concentration measurements with the Photoelectric counter are accurate to within 10%.

The photocell current was amplified so that I and I_0 could be recorded on a digital voltmeter (of 0 - 200mV range) with a paper-tape printout. The amplifier circuit used is shown in figure 3.2.

The 820 Ω resistor across the output of the amplifier effectively converts the variable current output to a 0 - 200mV voltage output, suitable for the digital voltmeter. The linearity of the amplifier's voltage output was tested by varying the current to the lamp supply, and plotting the direct photocell output versus the voltage output recorded on the digital voltmeter. This plot is shown in figure 3.3, verifying that the choice of resistors gives a linear output with sufficient gain over the range of interest.

FIG. 3.2 THE INVERTING AMPLIFIER

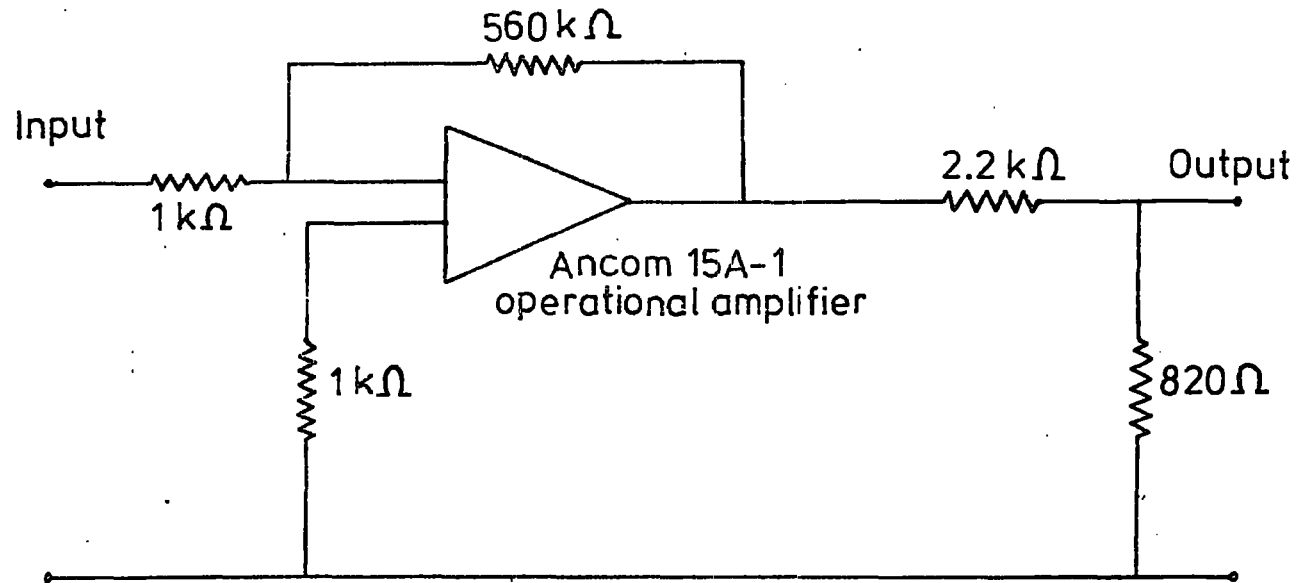
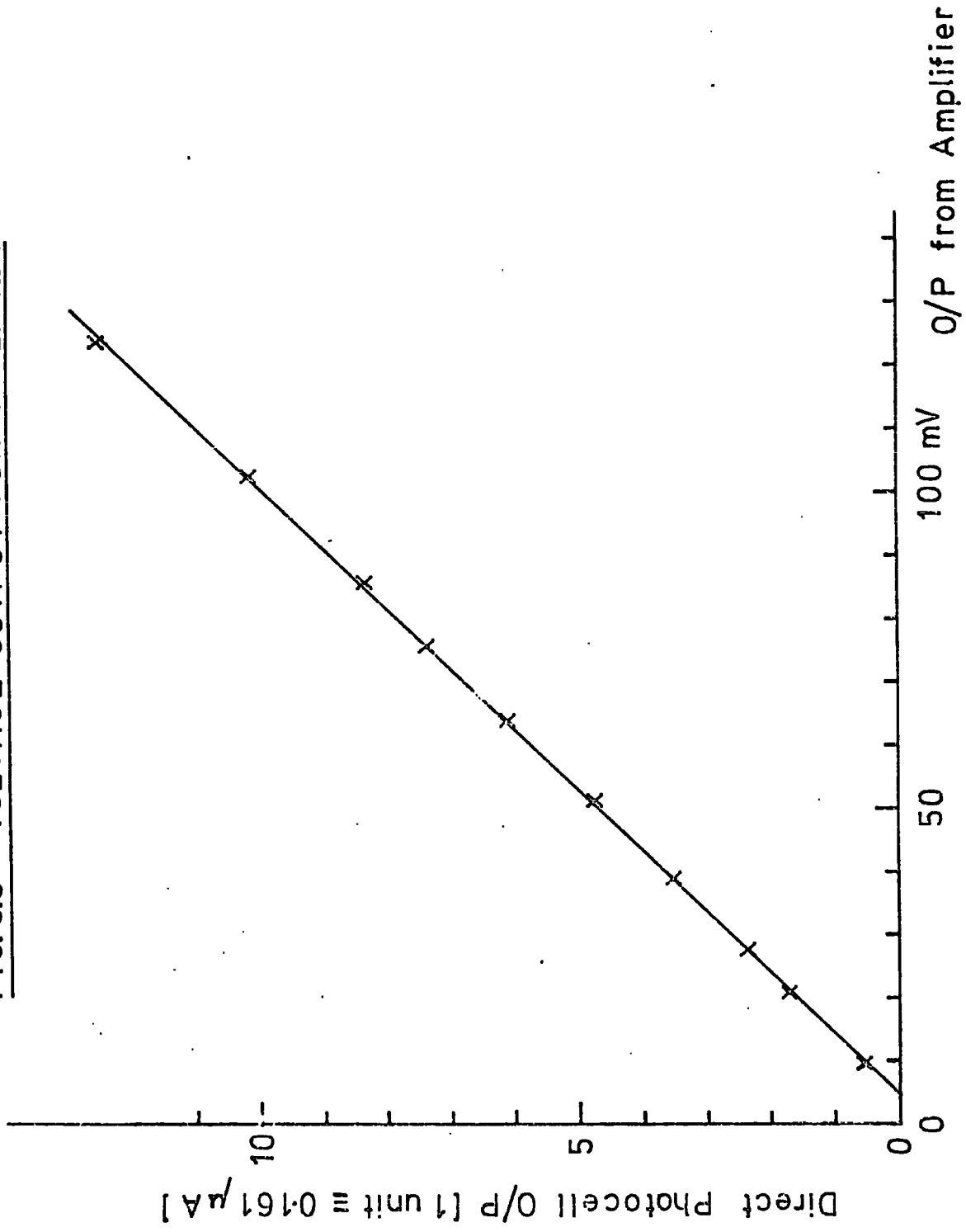


FIG. 3.3 VOLTAGE OUTPUT FOR AMPLIFIER



It was necessary for all experiments to have an automatic system for concentration measurements, and hence all the electrically operated solenoid valves, the galvanometer and the digital voltmeter were connected to a Rotaset programme timer, with a two minute cycle time. The cams on the timer discs were adjusted to give the following mode of operation :

TIME (secs)	FUNCTION OF TIMER	OPERATION
0	open valves 1 and 2	air sample drawn through counter using pump, flow measured with rotameter
58	close valves 1 and 2 open valve 3	filtered air pumped in until required overpressure is reached (160mm Hg)
67	close valve 3	
81	photocurrent to D.V.M.	
86	trigger D.V.M.	record I_0
86.5	open valve 4	sudden expansion
90.0	trigger D.V.M.	record I
100	current from photo-cell cut off	
112.5	close valve 4	
120	reopen valves 1 and 2	(cycle repeats)

The valve numbers here refer to diagram 3.1. These timings comply with the necessary conditions stated by Nolan and Pollak for satisfactory operation of the counter. The time between the expansion and the second trigger of the D.V.M. was fixed so as to give the minimum extinction reading, and was equal to 3.5 seconds.

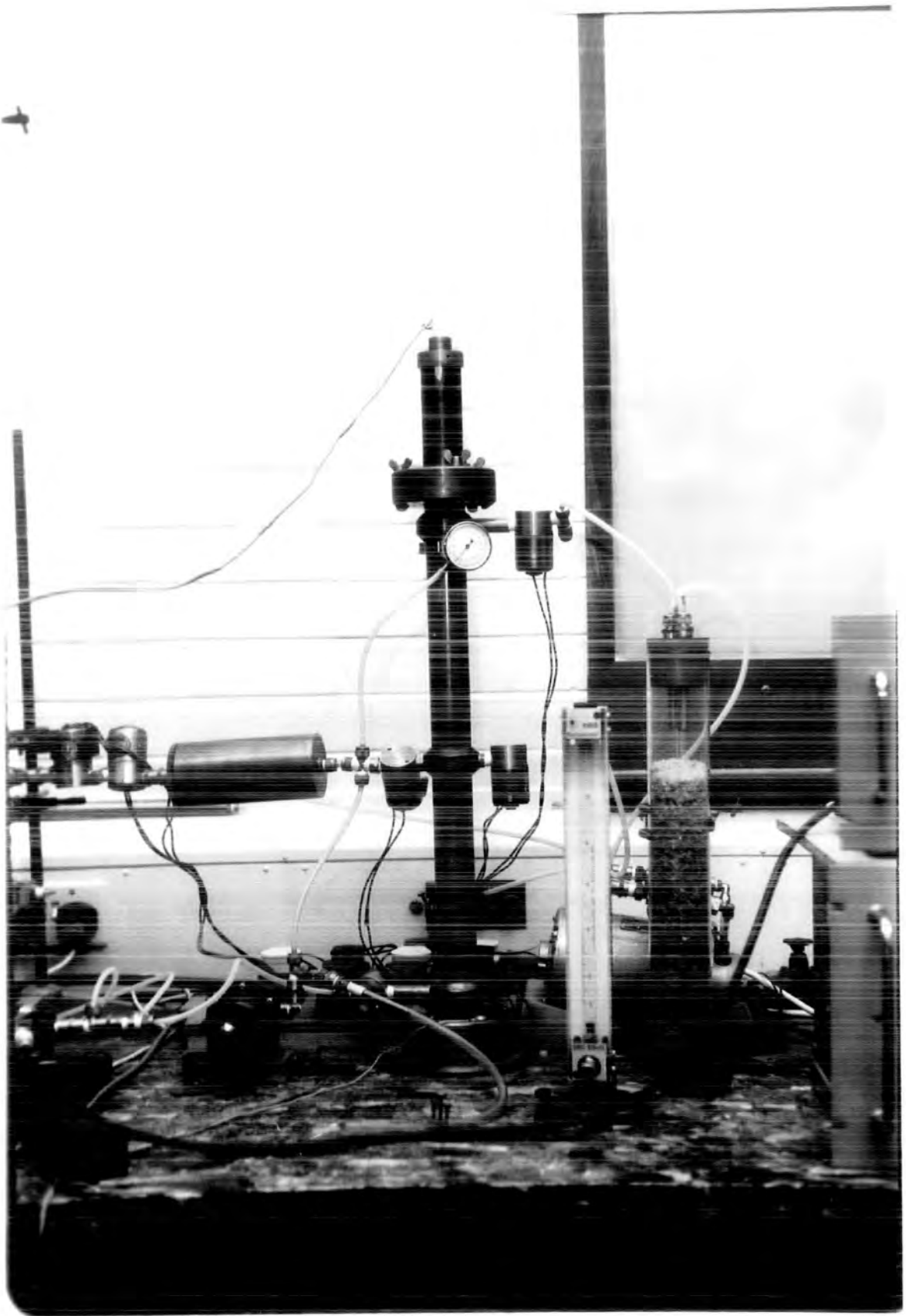


PLATE 2. The Photo-electric Counter System.

With the counter operating continually in this mode, and with an average air flow-rate of 5 litres per minute through the counter during the first half of each cycle, it was necessary to remoisten the blotting paper in the counter every 20 hours, to ensure that each sample became saturated with water vapour.

All metal to metal screw- thread connections to the counter were sealed with P.T.F.E. tape, and the counter system was tested for leaks before commencement of use. Plate 2 shows the assembled counter system.

3.3 The Measurement of Size of Sub-micrometre Aerosol Particles by the Diffusion Battery Method.

The relation between the fraction of aerosol particles penetrating a series of narrow channels and the diffusion coefficient of the particles was first investigated by Townsend (1900), and was first applied to atmospheric particles by Nolan and Guerrini (1935) using a diffusion battery containing a number of parallel rectangular channels. Timoney, working with Nolan and Guerrini, developed an equation for the diffusion loss of particles in the parallel plate battery which was later corrected by Gormley in an appendix to a paper by Nolan and Nolan (1938). If the particle concentration entering the box is Z and the concentration emerging from the box is Z_v , then:

$$\frac{Z_v}{Z} = 0.910 e^{-\alpha} + 0.053 e^{-11.4 \alpha} + \dots \quad (3.1)$$

where $\alpha = \frac{3.77 b D L C}{a Q} = \frac{D}{k Q}$

Here Q is the volumetric flow rate, C the number of channels, $2a$ the spacing between the parallel plates, b the height of the channels perpendicular to the direction of air flow, L the length of the diffusion tube and D the diffusion constant of the aerosol particles. The quantity k is a constant for a given box. Two diffusion batteries were used for this work: the battery for larger size aerosol particles (in the $1 - 5 \times 10^{-6}$ cm range) had $k_1 = 5.704 \times 10^{-7} \text{ cm}^{-1}$, whereas the battery for the smaller size range ($0.25 - 1 \times 10^{-6}$ cm) had $k_2 = 8.545 \times 10^{-6} \text{ cm}^{-1}$.

The discussion above refers to monodisperse aerosols, whereas most aerosols are polydisperse. Pollak and Metnieks (1957, 1959) found that when using the Nolan and Guerrini method to measure the diffusion coefficient for polydisperse aerosols, the values of D calculated by means of equation (3.1) from experimental observations increased with the rate of flow. These authors proposed to make use of this result for the determination of the size distribution of the heterogeneous aerosol (from the distribution of diffusion coefficients). The aerosol is resolved into a number of discrete size components by using the so called 'exhaustion' method, which is described in their 1957 paper. This lengthy procedure was not adopted in this work, for several size determinations were required here.

Natural aerosols and aerosols in the laboratory are commonly found as a continuous size distribution of particles which follows a log-normal probability law, where the probability density is given by:

$$Y = \frac{1}{(\ln \beta_g) \sqrt{2\pi}} \exp. \left[\frac{-(\ln r - \ln r_g)^2}{2 \ln^2 \beta_g} \right] \quad (3.2)$$

where r_g is the geometric mean size and β_g is the geometric standard deviation. Megaw and Wiffen (1963) showed experimentally (using electronmicro-photographs) that aerosols produced by atomising a 0.1% solution of potassium permanganate and allowing the drops to evaporate, and by heating a tungsten wire to a temperature of 1000-1200°C in a current of filtered nitrogen both closely followed a logarithmic probability law. For such an aerosol only the parameters r_g and β_g are needed to define the size distribution.

Fuchs et al. (1962) have devised an indirect method by which these two parameters can be obtained with the diffusion battery. They used the penetration equation of DeMarcus (1952) as a starting point:

$$\frac{Z_v}{Z} = 0.9149 e^{-1.885\alpha} + 0.0592 e^{-22.33\alpha} + 0.026 e^{-151\alpha} \quad (3.3)$$

Using an electronic computer they plotted a system of curves $Z_v/Z = f(y)$ (where $y = 1/kQ$) for aerosols having a logarithmic probability distribution, so that experimental values of Z_v/Z could be compared with them. This was done for several values of the mean geometric particle radius r_g from 10^{-7} to 10^{-5} cm, and for values of β_g from 1 (corresponding to a monodisperse aerosol) to 2.5. These curves are shown in figure 3.4, which is copied from Fuchs's paper. (Here n/n_0 corresponds to Z_v/Z , and $\log 1.8852y = \log (1/kQ)$). Millikan's equation (1923) was used to relate the diffusion coefficients to

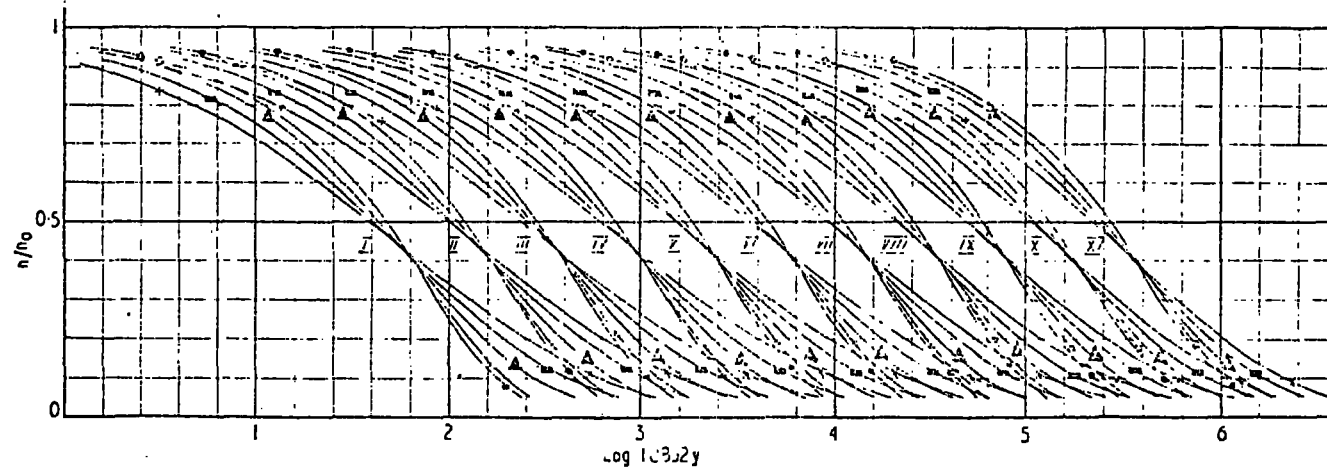
the particle radii, on the assumption that the particles are spherical:

$$D = \frac{kT \left(1 + A\lambda/r + B(\lambda/r) e^{-Cr/\lambda} \right)}{6\pi\eta r} \quad (3.4)$$

where $\lambda = 6.53 \times 10^{-6}$ cm is the mean free path of the air molecules, $\eta = 1.83 \times 10^{-4}$ dyn s cm⁻² is the viscosity of the air (at 23°C and 760mm Hg), $A = 1.246$, $B = 0.42$ and $C = 0.87$. These values were found by Millikan for oil droplets. There is a variation in the value of the constants with the nature of the droplet (Millikan, 1923; Wasser, 1933). However the uncertainty in the value of the particle radius due to this variation does not exceed 2-3%.

The important feature of Fuchs's method is that each family of curves for a particular r_g and varying β_g intersect when Z_v/Z has a value between 0.4 and 0.45. Hence if the air-flow through the diffusion battery is adjusted such that the value of Z_v/Z is between these values, then the radius obtained with this flow-rate will be the geometric mean radius of the aerosol. β_g and r_g can be obtained for a particular aerosol under study by determining values of Z_v/Z for three different air-flows, (with one value between 0.4 and 0.45). The results are plotted on tracing paper with Z_v/Z as abscissa, $\log(1/kQ)$ as ordinate, and having the same scale as figure 3.4. Comparison of these points with the theoretical families of curves then yields values of β_g and r_g . Megaw and Wiffen (1963) report that good agreement has been found in experiments in which the geometric mean size of various aerosols as given by Fuchs's method has been compared with that obtained from electronmicrophotographs of samples of the aerosols. The Fuchs method has been used in this work for all determinations of aerosol size. Figure 3.5

DETERMINATION OF PARTICLE SIZE DISTRIBUTION IN POLYDISPERSE AEROSOLS BY THE DIFFUSION METHOD



Penetration curves of polydisperse aerosols through a parallel-walled channel.

Curves	I	II	III	IV	V	VI
r_g (cm)	10^{-7}	1.6×10^{-7}	2.5×10^{-7}	$4 \cdot 10^{-7}$	6.3×10^{-7}	10^{-6}
	VII	VIII	IX	X	XI	
	1.6×10^{-6}	2.5×10^{-6}	$4 \cdot 10^{-6}$	6.3×10^{-6}	10^{-5}	
Symbols	•	○	▲	■	×	
$\text{Log } \beta_g$	0	0.1	0.2	0.3	0.4	

FIG. 34

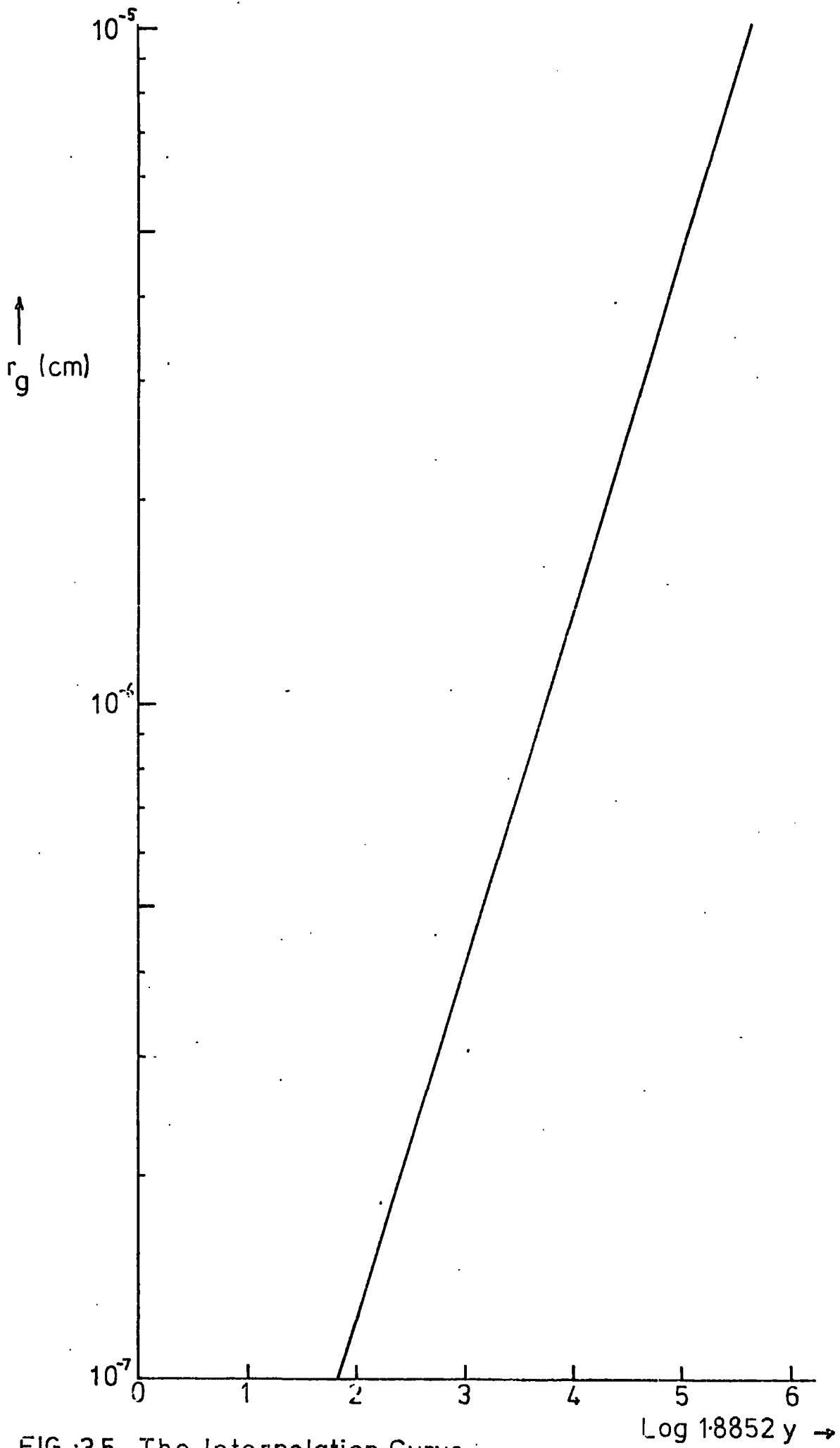


FIG. 3.5 The Interpolation Curve.

shows the extrapolation curve used between Fuchs's values of the radius, to determine the intermediate radius values.

3.4 Ion-tube Measurements on Charged Particles.

When large ion equilibrium exists in aerosols, due to frequent collisions with small ions, then the Boltzmann distribution law can be applied to the nuclei if the electrical energy is included. Keefe, Nolan and Rich (1959) have shown that under these conditions:

$$\frac{Z}{N_0} = \sqrt{\frac{2\pi KT}{p^2}} \quad (3.5)$$

where Z is the total number of aerosol particles per unit volume, N_0 is the total number of uncharged particles per unit volume and p is the number of charges per particle. Experimental results of Nolan and Kennan (1949) for values of Z/N_0 for nuclei of different sizes produced from hot platinum give good agreement with this hypothesis.

A conventional ion-tube is normally used to measure the ratio Z/N_0 . The ion-tube used for for this work is shown in figure 3.6. The mode of action of the ion-tube is well described in a paper by T.A.Rich (1959). Using b and h as defined in the diagram, the critical mobility at which all charged particles passing through the tube are captured is given by:

$$\omega_c = \frac{Qh}{lbV} \quad (3.6)$$

where Q is the flow rate in $\text{cm}^3\text{sec}^{-1}$, and V is the voltage across the

$h = \text{spacing between plates} = 0.314 \text{ cm}$
 $b = \text{mean circumference} = 12.80 \text{ cm}$
 $l = 85.34 \text{ cm}$

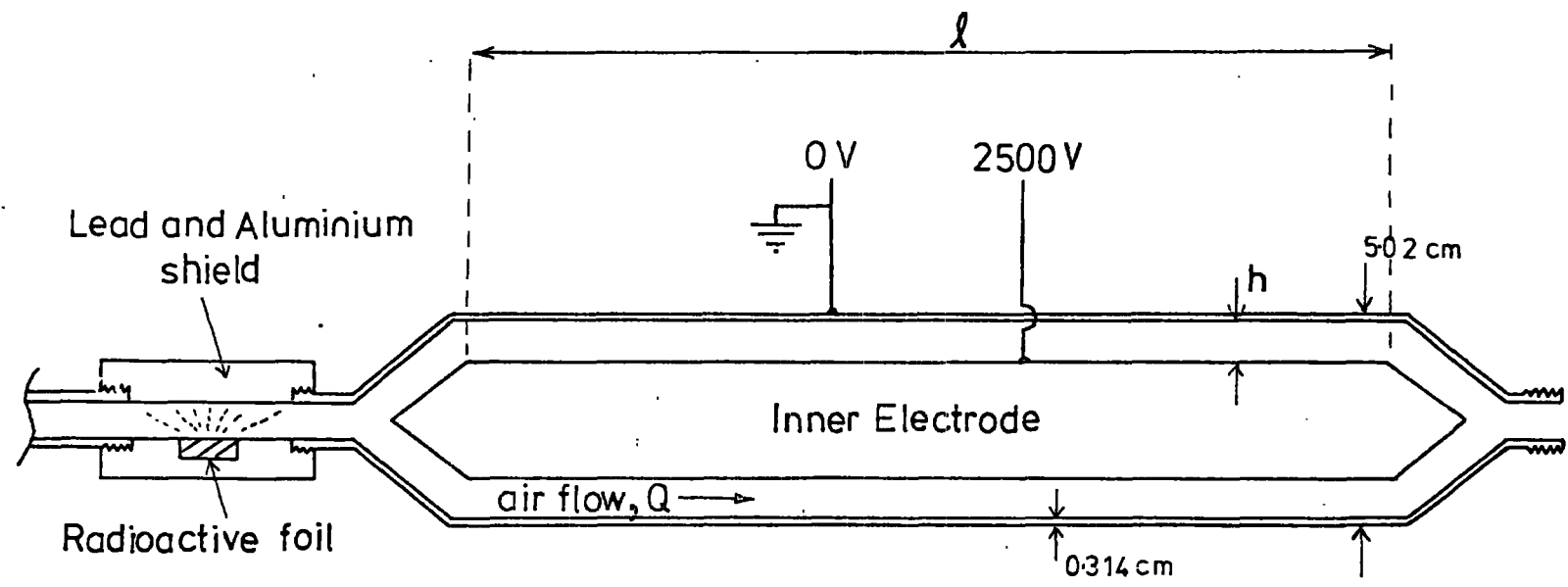


Fig. 3.6 Schematic Diagram of the Large Ion Tube.

plates. A voltage of 2.5kV was chosen in the experiments. This ensured that all singly charged particles with radii less than 1.5×10^{-4} cm were captured with a flow rate of 3 litres per minute, using the tables of Flanagan and Tayler (1967). An Americium α foil source of strength 125 μ C (shown in figure 3.6) was placed in line to ensure that the aerosol under study was in charge equilibrium. Tests were made to make certain that the α -source did not produce condensation nuclei. With the α -source in line, the ion-tube was used for measuring $(N_o/Z)_\infty$. The equivalent radius of nuclei could then be determined using the tables of Metnieks and Pollak (1961) for $(N_o/Z)_\infty$ versus radius. Preliminary experiments showed that the value of the equivalent radius measured with the ion-tube differed by only 5% from the value of the geometric mean radius measured by the diffusion battery.

In this work, the ion-tube was primarily used to measure (N_o/Z) . The diffusion battery method was used for size determination, (giving more accurate values of size for $r < 1.0 \times 10^{-6}$ cm) from which $(N_o/Z)_\infty$ could be determined from Metnieks and Pollak's tables. Hence for the majority of time, the α -source was removed, and the ion-tube - in conjunction with the diffusion battery - was then capable of measuring the departure of the aerosol from charge equilibrium. This procedure was adopted for the measurement of η_o versus radius, outlined in the next section of this chapter.

3.5 Experimental Determination of b versus radius and η_o versus radius.

Now that an experimental value for α had been obtained, and having checked that the photo electric counter, the diffusion battery

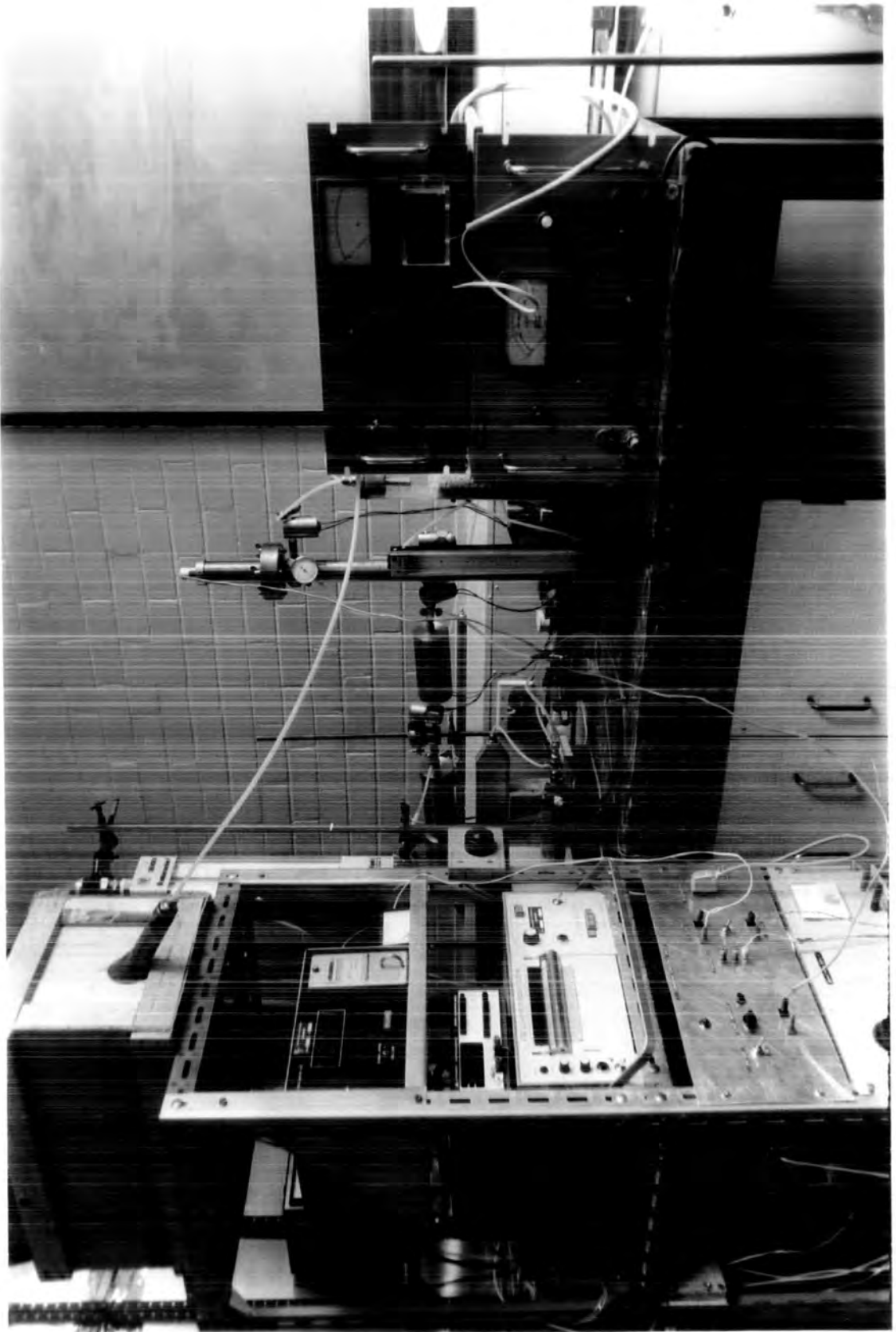


PLATE 3. Electrical Instrumentation associated with the Experimental System.

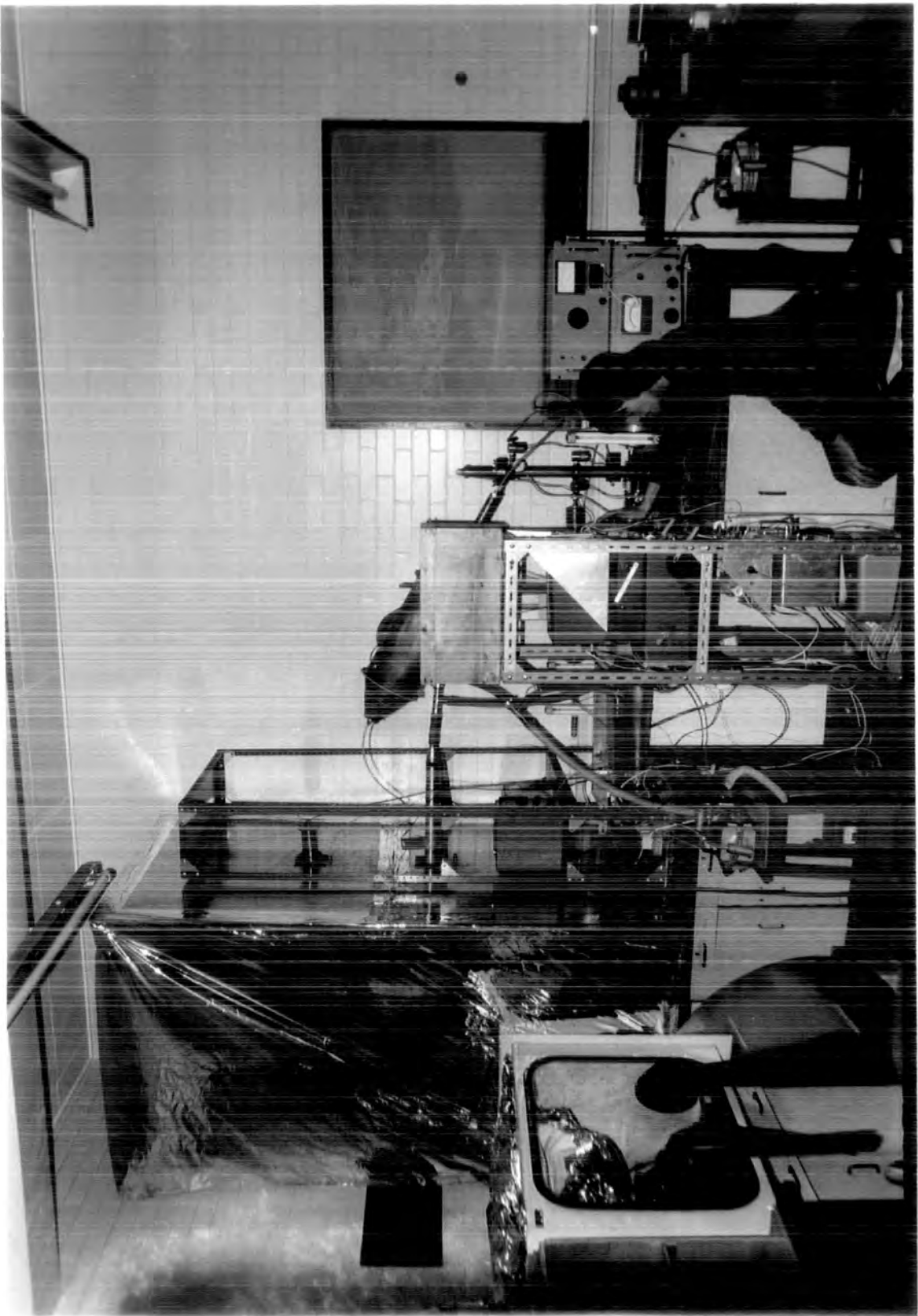
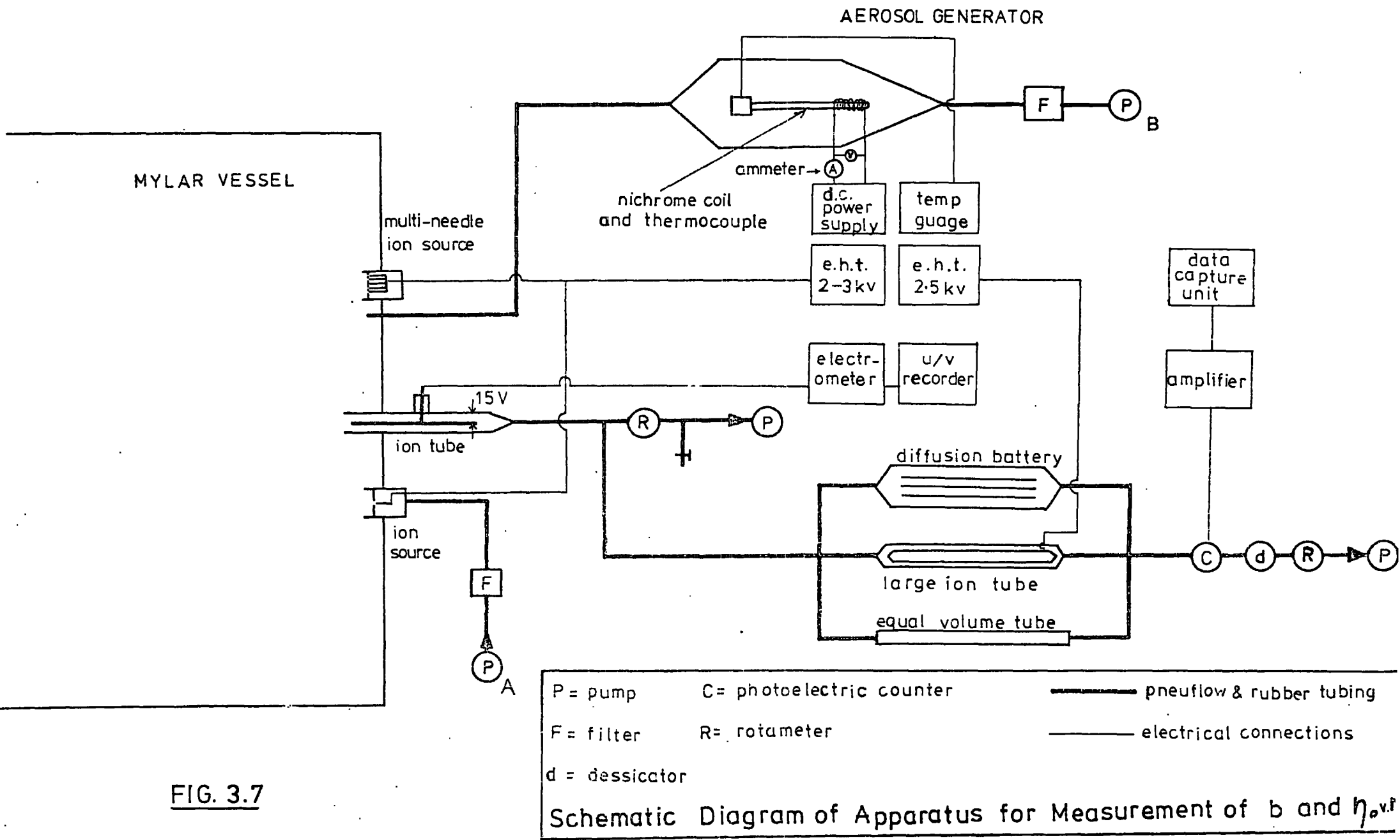


PLATE 4. A General View of the Experimental System.

and the ion-tube were working satisfactorily, the main set of experiments in this work were ready to be performed. The lay-out of the apparatus for this is shown in figure 3.7 and in the two photographs, plates 3 and 4. Inter-connecting pneuflow $\frac{1}{4}$ " tubing was made as short as possible to minimize diffusion losses. As with the α determination, the aerosol particles were initially drawn through the small ion-tube and then through 1" diameter rubber tubing to the rotameter and pump. The flow rate employed was 50 litres per minute. The sample line to the counter, through the diffusion battery or large ion-tube or equal volume tube (to the diffusion battery) was all of $\frac{1}{4}$ " pneuflow tubing, connected to the main sample line from the mylar vessel by a 'Y' piece. (It should be noted here that rotameter readings through the small ion-tube were only made with no flow of air through the photo-electric counter, so that one junction of the 'Y' was effectively blocked.) The choice of routes to the counter was determined by two-way electrical solenoid valves.

For measuring b versus radius the following procedure was adopted. The mylar vessel was filled with filtered air using pump A. Aerosol particles were introduced into the vessel using pump B with a 40 litres per minute flow rate. If small particles were required, then filtered air from pump A was used to fill the vessel for the majority of the time, with aerosol production using pump B only for the last few minutes before the vessel was full. This production time for small particles of size ranging from 0.5 to 1.0×10^{-6} cm varied from two to twenty minutes. If large particles were required, then the aerosols were produced for a much longer time; from one hour duration for particles $\sim 2.0 \times 10^{-6}$ cm upto 80 minutes for the largest particles obtained. For the large particles the amount of filtered air pumped



into the vessel was reduced, and for the largest particles no filtered air was pumped into the vessel from pump A. It should be mentioned here that the current through the nichrome wire was varied for different size requirements as indicated in section 3.1.

Concentration measurements were then made every two minutes on samples of the aerosol. The aerosol was stored for a period depending on the size required for each experiment. For small particles this was between 10 and 20 minutes, and for larger particles for more than an hour. During this time, air was passed through the diffusion battery with trial flow rate values to determine which flow reading would give a value of Z_v/Z of between 0.4 and 0.45. The size was then determined accurately using the following analysis scheme, with concentration readings every two minutes:

- | | | | |
|-----|-------|---|--|
| (1) | Z | } | measurement with airflow through equal volume tube. |
| (2) | Z | | |
| (3) | Z | | |
| (4) | Z_v | } | measurement through diffusion battery with same flow rate as for (1), (2) and (3). |
| (5) | Z_v | | |
| (6) | Z_v | | |
| (7) | Z | } | measurement with airflow through equal volume tube. (same flow rate). |
| (8) | Z | | |
| (9) | Z | | |

For the very small particles there was often insufficient time before reading (1) to find the correct flow rate for Z_v/Z to be ~ 0.4 ,

so it became necessary to perform a preliminary experiment to obtain this value. After flushing with filtered air, the vessel would again be filled using exactly the same parameters for aerosol production as in the trial run, and then the main experiment could be carried out, using the flow rate value previously obtained. The geometric means of the six Z and three Z_v readings were taken to give the ratio Z_v/Z , generally around 0.42; the size measurement was rejected if the ratio was outside the limits of 0.34 and 0.50. Immediately after the last Z measurement (number(9)) small ions were pumped into the vessel from the lower ion source for a time long enough for the ion concentration inside (measured on the U/V recorder connected to the small ion-tube via the Keithley electrometer) to be above 4000 ions per cm^3 . Then the flow rate to the needle was stopped and the decay of ions inside the vessel was recorded on the U/V paper, as in the method for determining α , outlined in Chapter 2. When the ions had reached equilibrium, aerosol concentration measurements were again taken and another size measurement made, identical as before. It was not possible to make aerosol concentration readings during the ion decay time as the electro-magnetic valves interfered with the electrometer when they were switched on or off. A check on the value of n_∞ was made five minutes after completion of the decay run. The decay time (from n_0 to n_∞) varied between two and six minutes, so there was no appreciable gap of time between the two size determinations, and in most cases increase of size over this time due to coagulation was minimal. For experiments where some coagulation was found to occur the flow rate through the diffusion battery was reduced slightly for the second size determination. Geometric means were again taken to evaluate the average size and concentration during the decay of the ions.

An experimental decay run is shown in figure 3.8. The initial ion concentration corresponding to $t = 0$ was chosen to be 4000 ions per cm^3 . The geometric mean size for this aerosol sample was found to be 2.02×10^{-6} cm, and the average concentration of nuclei during the run was 13,810 particles per cm^3 . The corresponding set of theoretical curves for this decay, plotted by computer, is shown in figure 3.9. These curves represent a plot of the solution (1.16) of $\frac{dn}{dt} = q - \alpha n^2 - \beta n$ for values of β from 0.005 to 0.050 (in steps of 0.005). Families of curves as in figure 3.8 were plotted for a particular value of n , ranging from $n_{\infty} = 100$ ions per cm^3 to 1500 ions per cm^3 , at 50 unit intervals. (For the larger values of n_{∞} , the values of β plotted were from 0.001 to 0.015, at 0.001 intervals. These sets of curves correspond to the decay of ions in samples of small sized particles, where the value of β will also be relatively small unless the concentration of particles was very large, which did not apply in any of the experimental runs.) Figure 3.9 is the theoretical set of curves with the value of n_{∞} closest to that obtained experimentally in figure 3.8. A comparison of the experimental decay curve with the family of curves for the first two minutes gives a value of β of 0.034. From the relationship $\beta = bZ$, b is then determined to be $2.46 \times 10^{-6} \text{ cm}^3 \text{ sec}^{-1}$. The error in b was evaluated from the error in β and the error in Z . The error in β was estimated from the fluctuation of the experimental decay curve from the theoretically computed curves. The error in Z was taken as 8% for all experiments, corresponding to the accuracy of the photo-electric counter. For the above quoted b value the error was found to be $\pm 0.27 \times 10^{-6} \text{ cm}^3 \text{ sec}^{-1}$.

For the measurement of γ_0 versus radius one extra measurement has to be introduced in the experiment, that of the number concentration of uncharged particles, N_0 . This is achieved using the ion-tube.

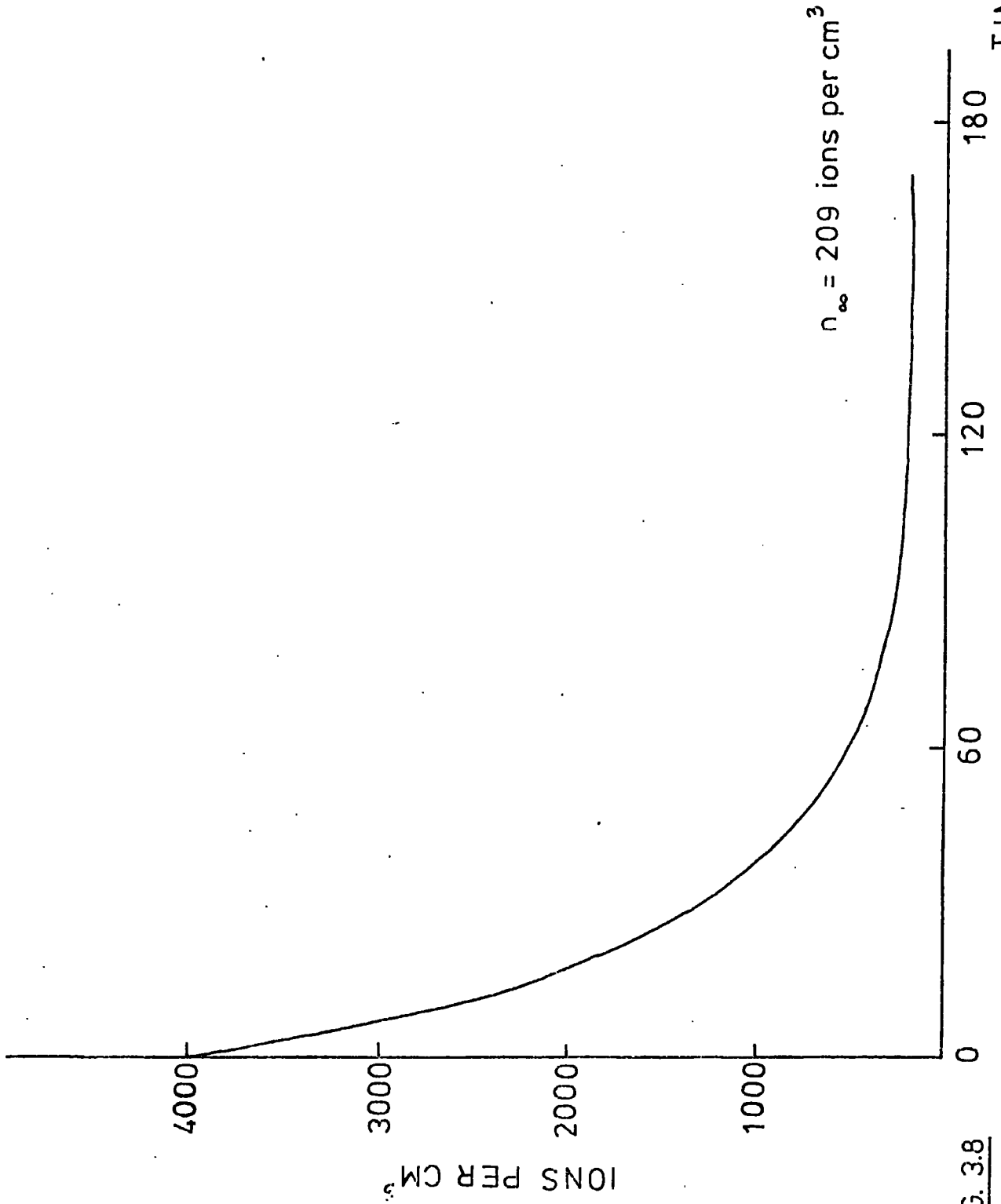


FIG. 38

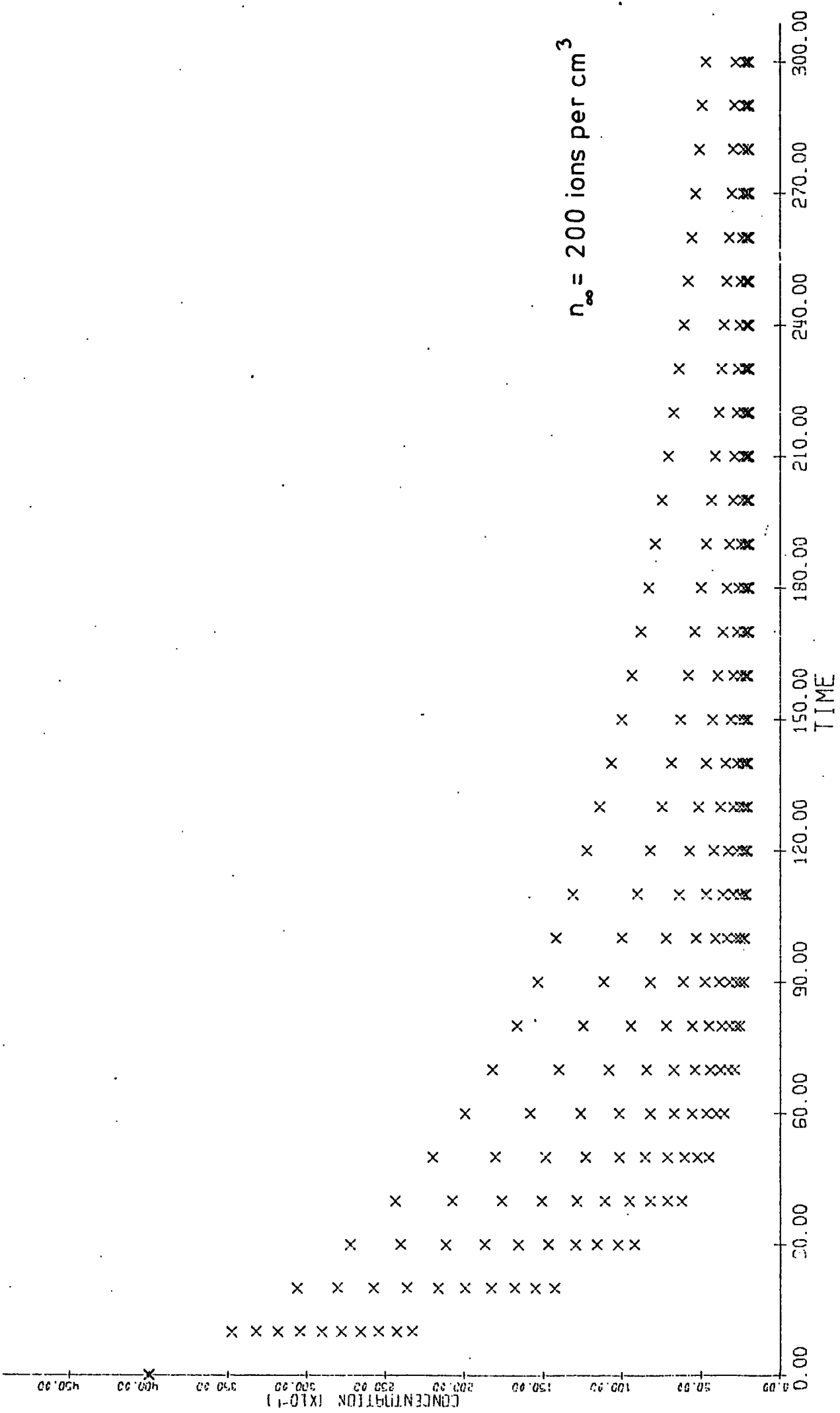


FIG. 3.9

as indicated in section 3.4. The analysis scheme for η_0 measurement was as follows:

- | | | | |
|------|----------------|---|---|
| (1) | Z | } | measurement with airflow through the equal volume tube. |
| (2) | Z | | |
| (3) | Z | | |
| (4) | Z _v | } | measurement through diffusion battery, with same flow rate as for (1), (2) and (3). |
| (5) | Z _v | | |
| (6) | Z _v | | |
| (7) | Z | } | measurement with airflow through equal volume tube, (same flow rate). |
| (8) | Z | | |
| (9) | Z | | |
| (10) | N _o | } | measurement with ion-tube, (same flow rate). |
| (11) | N _o | | |

Ion decay measurement.

Stages (1) to (11) in reverse order.

The geometric mean value of N_o was found, corresponding to the average value during the decay. b was determined using the method described above, and then η_0 could be calculated from equation (1.20), where f and l values were determined from the measured values of (N_o/Z) and $(N_o/Z)_\infty$ using the ion-tube and diffusion battery respectively.

The full results of b versus radius and η_0 versus radius experiments are tabulated in chapter 5, where they are also plotted graphically.

*

*

*

CHAPTER 4.

THEORETICAL CALCULATIONS OF COMBINATION COEFFICIENTS.

Combination coefficients between small ions and aerosol particles have been well studied for the situation when the radius of the particle is larger than the ionic mean free path, using the diffusion-mobility equation:

$$r^2 \left(D \frac{dn}{dr} + \frac{dU}{dr} Kn \right) = \text{const.} = \phi \quad (4.1)$$

(the ionic flux)

where D is the diffusion coefficient, K the mobility and n the concentration of small ions, and U is the electric potential at distance r from the centre of the particle, of radius a . Bricard (1949) made allowance for the image charge of the nucleus in the expression for the potential gradient, but his expressions for the combination coefficients required modification in the case of $a \lesssim$ the ionic mean free path. The same author in 1962 introduced the mean free path, λ , of the ions into the calculations by defining a "limiting sphere" of radius $\Delta + a$ concentric with the aerosol particle, where Δ is of the order of the size of the mean free path of the small ions. The small ions undergo their last collision outside this sphere, so that in the layer of thickness Δ the ions move around as if in empty space, travelling at the mean thermal velocity, \bar{c} . Smolukowski (1918) had calculated the value of Δ assuming that the departure of the diffusing small ions from the external surface is equally probable in all directions, and Bricard used his result for a value of Δ given by:

$$\Delta = \frac{1}{3\lambda a} \left[(a + \lambda)^3 - (a^2 + \lambda^2)^{3/2} \right] - a \quad (4.2)$$

which gives $\Delta = \lambda$ for small a , and $\Delta = \lambda/2$ for ' a ' very large. Outside the sphere of radius $\Delta+a$ the diffusion-mobility treatment holds, whereas inside the sphere collision treatment of kinetic theory is applicable. The ionic flux ϕ_a reaching the particle is:

$$\phi_a = \pi a^2 \bar{c} n_{a+\Delta} \quad (4.3)$$

where $n_{a+\Delta}$ is the small ion concentration at the outer surface of the shell. At equilibrium:

$$\phi_a = \phi_{a+\Delta} \quad (4.4)$$

Bricard substituted the R.H.S. of equation (4.4) in the diffusion-mobility equation (4.1) and obtained the coefficients η_{1p} and η_{2p} (of nuclei carrying elementary charges of the same sign as of the small ions and of opposite sign respectively) in a similar way to his previous method.

$$\left. \begin{aligned} \eta_{1,p} &= \frac{\pi a^2 \bar{c} p \frac{e^2}{kT} \exp \frac{-pe^2}{kT(a+\Delta)}}{p \frac{e^2}{kT} + \frac{\bar{c}}{4D} a^2 \left[1 - \exp \frac{-pe^2}{kT(a+\Delta)} \right]} \\ \eta_{2,p} &= \frac{\pi a^2 \bar{c} p \frac{e^2}{kT} \exp \frac{pe^2}{kT(a+\Delta)}}{p \frac{e^2}{kT} - \frac{\bar{c}}{4D} a^2 \left[1 - \exp \frac{pe^2}{kT(a+\Delta)} \right]} \end{aligned} \right\} (4.5)$$

Bricard (1965) showed that in particular for uncharged particles the combination coefficient η_0 reduces to:

$$\eta_0 = \frac{\pi a^2 \bar{c}}{1 + \frac{\bar{c}}{4D} \frac{a^2}{a+\Delta}} \quad (4.6)$$

However, these modified values of the combination coefficient were evaluated with the simplification of neglecting the image charge.

Keefe, Nolan and Rich (1959) discuss how the ratios of the combination coefficients η/η_0 , η^{21}/η^{12} , η^{22}/η^{23} etc. (where η_0 is the combination coefficient for uncharged aerosol particles, η is the coefficient for collisions between singly-charged aerosol particles and ions of opposite sign, η^{21} is the coefficient for collisions which change doubly-charged to singly-charged particles and vice-versa for η^{12}) can be obtained by application of the Boltzmann distribution law; for under equilibrium conditions,

$$\frac{\eta}{\eta_0} = \frac{N_0}{N_1} \quad ; \quad \frac{\eta^{21}}{\eta^{12}} = \frac{N_1}{N_{11}} \quad (4.7)$$

where N_0 , N_1 and N_{11} are the number concentrations of uncharged, singly and doubly charged particles respectively. Keefe and Nolan (1961) extended this study to the influence of image forces on the combination coefficient η_0 of small ions with uncharged aerosol nuclei. They considered three cases for different ranges of radius, a , of the nuclei; (i) $a > \lambda$, (ii) $a < \lambda$ and (iii) $a \sim \lambda$. Size ranges (ii) and (iii) are of more relevance here. When the size of the uncharged particles is much smaller than the mean free path of the small ions, the effective capture cross-section is enhanced beyond the geometrical size due to the attraction of the image charge. With this consideration, Keefe and Nolan obtained the following equation, assuming a Maxwellian velocity distribution of the small ions:

$$\eta_0 = \pi a^2 \bar{c} \left(1 + \sqrt{\frac{\pi e^2}{2 a k T}} \right) \quad (4.8)$$

In the case where a is of the order of λ (typical of atmospheric nuclei) the volume around the nucleus is split into two regions, as described earlier. η_0 is then modified as:

$$\eta_0 = \frac{\pi a^2 \bar{c} \left(1 + \sqrt{\frac{\pi e^2}{2 a k T}} \right)}{1 + a/\lambda'} \quad (4.9)$$

where λ' is the effective distance out from the nuclear surface to the boundary between the regions. For small radii ($< 10^{-6}$ cm) this equation tends toward the form of (4.8); for large radii ($> 10^{-5}$ cm) η_0 tends to $\pi\lambda'\bar{c}a$. λ' was evaluated by equating this asymptotic value to the result calculated for large nuclei in case (i), ($a > \lambda$); $\eta_0 = 4\pi ad$. Hence:

$$\eta_0 = \frac{\pi a^2 \bar{c} \left(1 + \sqrt{\frac{\pi e^2}{2a k T}} \right)}{1 + \frac{a \bar{c}}{4d}} \quad (4.10)$$

Keefe, Nolan and Scott (1968) extended the study on the effects of the image charge attraction to the combination of small ions and charged nuclei. Figure (4.1) shows the image capture sphere for the case when the small ion is attracted towards the nucleus. The radius of the image capture sphere, $s_0 a$, is the minimum apsidal distance for ion trajectories with corresponding impact parameter $b_0 a$. Orbits with impact parameter $b a > b_0 a$ will escape capture after passing through an apse, whereas those with $b a < b_0 a$ will spiral into the nucleus.

Ions move under an attractive force towards O: the central force. Hence the angular momentum of an ion about O remains constant. When the ion is at the apsidal distance, $s a$, the radial component of its velocity in the equation of conservation of energy becomes zero. Using this fact, and including the image force term in the potential energy expression, the following equation can be derived for charged spherical targets:

$$\frac{b^2}{s^2} = 1 \pm \frac{2pY}{s} + \frac{Y}{s^2(s^2-1)} \quad (4.11)$$

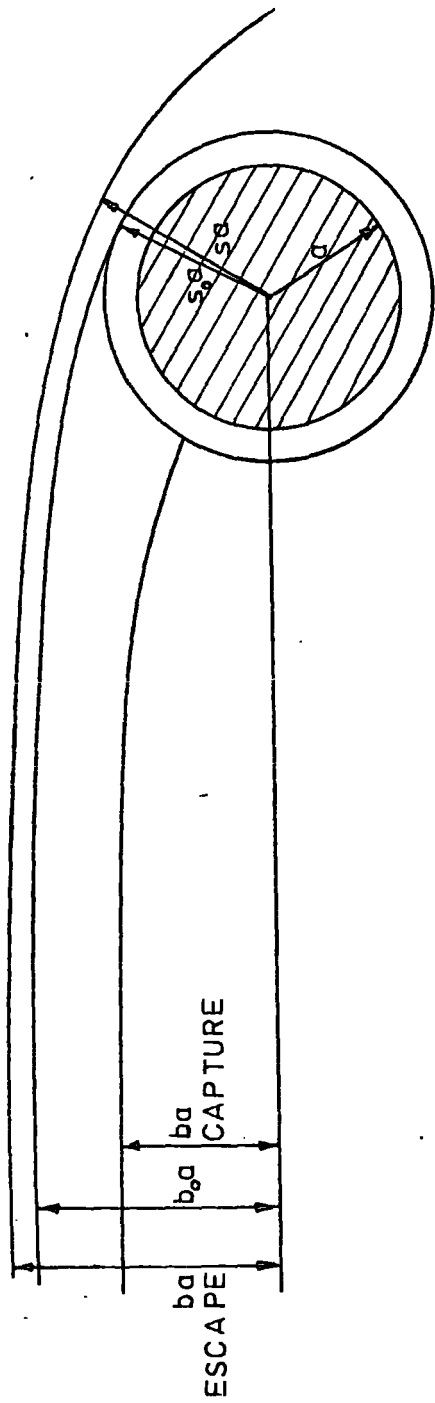


FIG. 4.1 ION TRAJECTORIES [ATTRACTIVE CASE]

where $Y = e^2 / amc^2$, b and s are the normalised impact parameters and apsidal distances respectively. p is the number of electronic charges on the nucleus and is negative for attraction. The minimum value of the larger root of this equation is that for the closest passing orbit which just escapes capture. This minimum value occurs when the two roots are equal; when $b = b_0$ and $s = s_0$, in diagram (4.1). In this situation the capture cross-section for ions approaching in a given direction with velocity c is enhanced to $\pi b_0^2 / \pi a^2$. The enhancement factor (denoted E.F.) is thus b_0^2 .

Keefe et al obtained values of b_0^2 from graphs of b^2 against s for various values of p and Y , and then plotted the enhancement factor (E.F.) against a , where a is deduced from Y , setting $\frac{1}{2}mc^2 = \frac{3}{2}kT$ (for $T = 290K$). Curves for $p = 1, 2$ and 3 were evaluated for both the attractive and the repulsive cases. These curves come together for large values of the radius, where the enhancement factor is approximately given by:

$$b_0^2 = 1 + 2\sqrt{Y} \quad (4.12)$$

This expression is also obtained for uncharged aerosol particles ($p = 0$), putting $db^2/ds = 0$ in equation (4.11): this result would be expected since the relative importance of the image force with respect to the coulomb force increases as the radius increases. Also for larger radii the geometric cross-section dominates over the electrical forces and hence the E.F. is small.

The variation of the normalised image capture distance, s_0 , with aerosol particle radius can be found directly from the minimum

condition of (4.11), where for the attractive case:

$$\frac{1}{Y} + \frac{p}{s_0} = \frac{1}{(s_0^2 - 1)^2} \quad (4.13)$$

and

$$Y = \frac{e^2}{3akT}$$

As $Y \rightarrow 0$, $a \rightarrow \infty$ and s_0 tends to unity; but for $Y \rightarrow \infty$, $a \rightarrow 0$, and $p(s_0^2 - 1)^2 \rightarrow s_0$, giving the endpoints of the attractive curves $s_0 = 1.49$ ($p=1$), $s_0 = 1.35$ ($p=2$) and $s_0 = 1.29$ ($p=3$).

To obtain realistic values of E.F. for various radii, Keefe et al. made an average over the Maxwellian velocity distribution of the small ions. Formulae were derived by trial from the single velocity b_0^2 values which had been evaluated over a wide range of Y values, as indicated earlier. Five values of p were included, and for the attractive case, the equation:

$$b_0^2 = 1 + (2p - \frac{1}{4})Y + 2\sqrt{Y(1 + pY)} \quad (4.14)$$

gave a fit to within 2%. The average enhancement factor using the Maxwellian small ion velocity distribution, $f(c)$, is expressed by:

$$E.F. = \frac{1}{c} \frac{\int_0^\infty c b_0^2 f(c) dc}{\int_0^\infty f(c) dc} \quad (4.15)$$

Substitution of b_0^2 values from (4.14) and integration gives:

$$E.F. = 1 + e^{py} \sqrt{y} \Gamma(\frac{1}{2}, py) + y(2p + 2\sqrt{p} - \frac{1}{4}) \quad (4.16)$$

for the attractive case, where $y = e^2/2akT$. The table 4.1 compares values of the enhancement factor evaluated by Keefe et al. (1968) from a single velocity (b_0^2) and those evaluated from the velocity distribution $\langle b^2 \rangle$, for the $p=1$ attractive case:

Table 4.1

$a \times 10^{-6} \text{cm}$	1	3	10	30	100
b_0^2	9.5	4.27	2.31	1.64	1.32
$\langle b \rangle^2$	12.5	5.29	2.61	1.75	1.35

A comparison of these two sets of results has shown that for small nuclei, integration over the Maxwellian velocity distribution can be replaced by using a single particle equivalent initial energy of $\frac{1}{2}mc^2 = kT$, whereas for large nuclei the equivalent initial energy turns out to be $1.25kT$.

For the special case of $p=0$, integration over the Maxwellian distribution gives:

$$E.F. = 1 + \sqrt{\pi y} \quad (4.17)$$

Equating (4.12) and (4.17) gives $\pi mc^2 = 8kT$, and hence the equivalent single velocity of the distribution is the mean velocity.

Hoppel (1974) compared the relative importance of image capture and three-body trapping, the latter effect being described in his 1969 paper. Both effects were then encompassed in a single theory and used to calculate values of the combination coefficients.

The three-body trapping distance, δ , is determined by the amount of kinetic energy lost by the ion approaching the nucleus in its last collision with a molecule: if the energy removed by the molecule is large enough, the ion will become trapped in the coulomb field of the nucleus. δ is defined as the average separation distance where the average energy removed from the ion by the third body is just

sufficient to ensure capture. Three-body trapping becomes important when δ is greater than $s_0 a$, the image capture distance. This does not occur for neutral nuclei, but for ions and nuclei with charge of opposite sign there is a critical nuclear radius below which three-body trapping becomes important.

Hoppel used a modification of Natanson's (1959) three-body recombination theory to determine empirical values of the ion-ion trapping distance for various atomic masses of the small ion. Natanson's expression for the ion-ion recombination coefficient can be written as:

$$\alpha = \frac{\pi d^2 f(q) \left(1 + \frac{e^2 \lambda}{d(d+\lambda) k_B T}\right) \exp\left(\frac{e^2}{(d+\lambda) k_B T}\right)}{1 + \frac{d^2 \bar{c}_r f(q) k_B T}{4 k e} \left(1 + \frac{e^2 \lambda}{d(d+\lambda) k_B T}\right) \left(\exp\left[\frac{e^2}{(d+\lambda) k_B T}\right] - 1\right)} \quad (4.18)$$

where k is the mobility, λ the mean free path, \bar{c}_r the mean relative velocity of the ions; d is the ion-ion trapping distance and $f(q)$ represents the probability that either ion suffers a collision while traversing the trapping sphere:

$$f(q) = 2\omega - \omega^2 \quad (4.19)$$

where: $\omega = 1 + 2 \left[\frac{e^{-q}}{q^2} + \frac{e^{-q}}{q} - \frac{1}{q^2} \right]$ and $q = 2d/\lambda$

Figure (4.2) gives the recombination coefficient as calculated from equation (4.18) as a function of trapping distance for several values of ionic mass. Values of the mean free path were found using the Langevin expression (1.5), with a value of $1.2 \text{ cm}^2 \text{ volt}^{-1} \text{ sec}^{-1}$ for k , and using a value of $4.58 \times 10^4 \text{ cm sec}^{-1}$ for \bar{v} , the average thermal

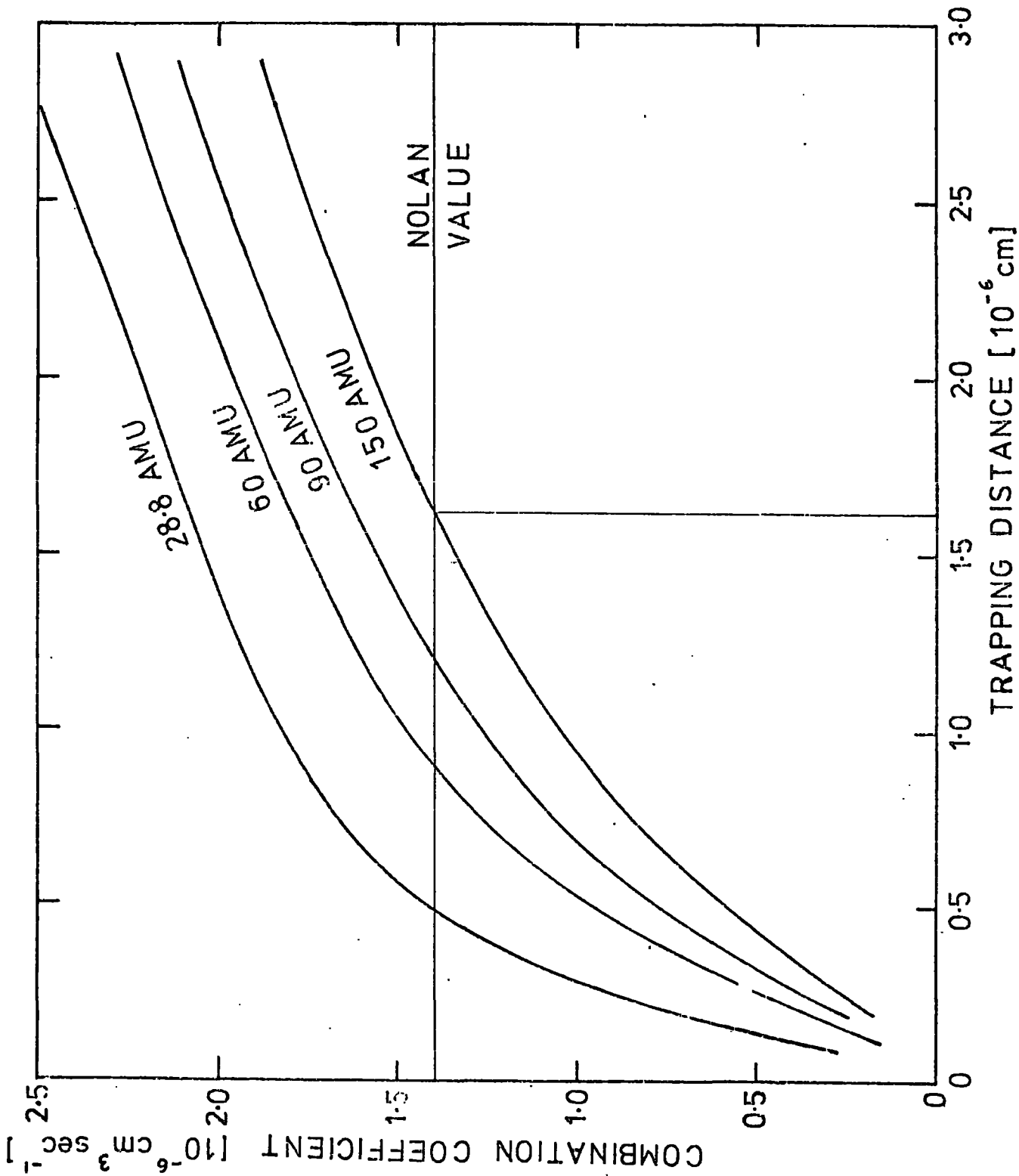


FIG. 4.2

velocity of the molecule. A value of 1.62×10^{-6} cm for the ion-ion trapping distance d was determined for calculations using Nolan's (1943) value for α and an atomic mass of 150 a.m.u.

The ion-aerosol particle trapping distance is determined from the ion-ion trapping distance by calculating the kinetic energy gained by one of the ions between the separation distances d and $d+\lambda$ (in the laboratory system):

$$E = \frac{e^2}{2} \int_{d+\lambda}^d \frac{dr}{r^2} = \frac{e^2}{2} \frac{d}{2d(d+\lambda)} \quad (4.20)$$

E gives the excess kinetic energy which an ion must possess if it is to lose sufficient energy upon collision with a molecule to ensure trapping. The ion-aerosol particle trapping distance δ is thus determined by:

$$\phi(\delta) - \phi(\delta + \lambda) = E \quad (4.21)$$

where the electrostatic potential energy $\phi(\delta)$, including both coulomb and image charge forces, is given by:

$$\phi(\delta) = \frac{pe^2}{\delta} - \frac{e^2 a^3}{2\delta^2(\delta^2 - a^2)} \quad (4.22)$$

Figure (4.3) shows the variation of δ with radius (determined by (4.21)) compared with the corresponding variation of $s_0 a$, determined by Hoppel using the substitution $\frac{1}{2}mc^2 = kT$. It is apparent from this diagram that the effect of three-body trapping is important for aerosol particle radii below about 2.0×10^{-6} cm, but can be ignored above this value.

Hoppel applied a collision treatment inside the sphere of radius

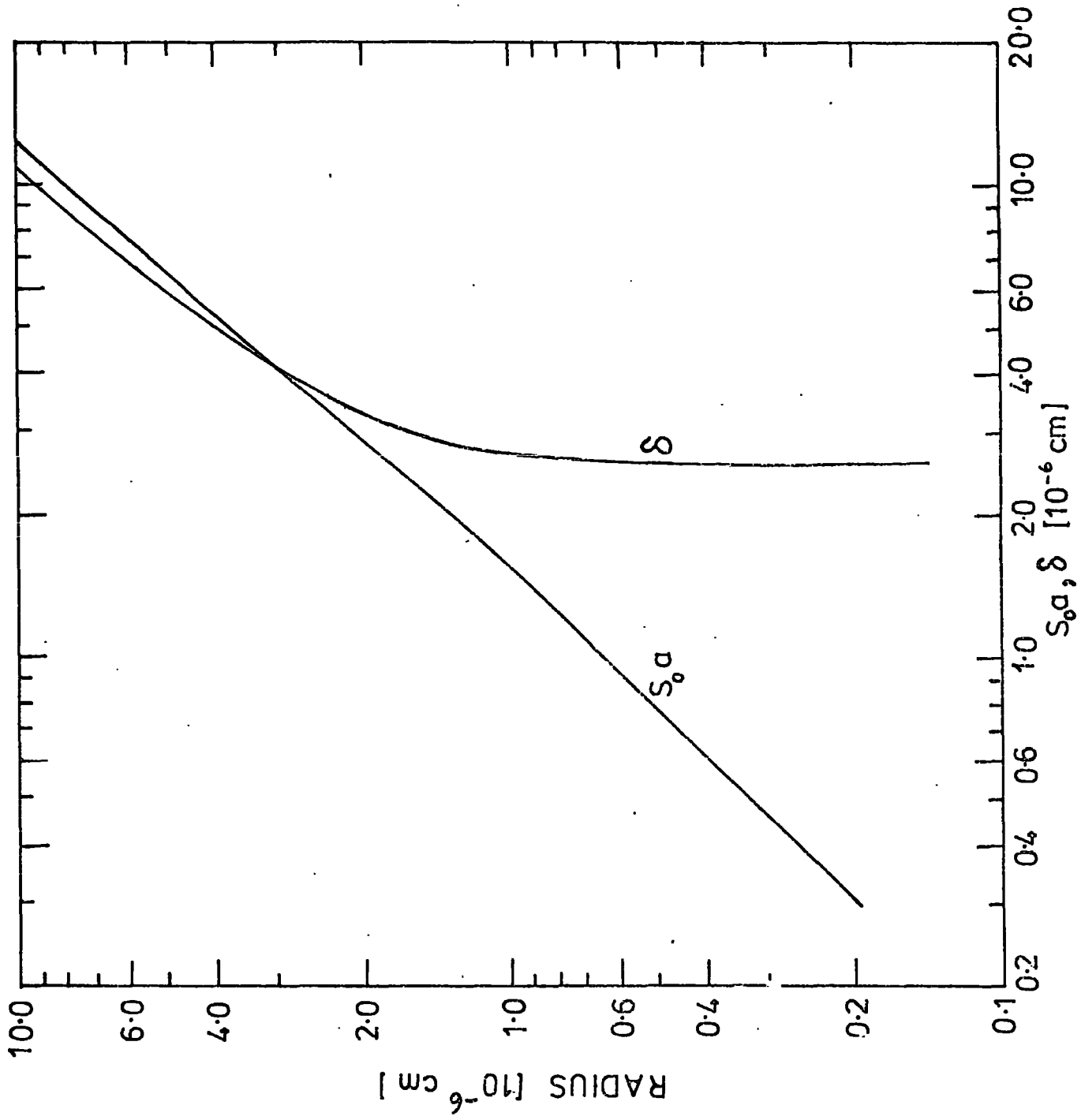


FIG 4.3

$\delta + \lambda$ to compute the flux of ions I_δ , entering the δ -sphere, and found:

$$I_\delta = \gamma \pi f(x) \delta^2 \bar{c} n_{\delta+\lambda} \quad (4.23)$$

where \bar{c} is the average velocity, γ is the enhancement of ions entering the δ -sphere resulting from electrical forces:

$$\gamma = 1 - \frac{\phi(\delta) - \phi(\delta + \lambda)}{kT} \quad (4.24)$$

$f(x)$ is the total probability that an ion passing through the δ -sphere will be captured, and is given by:

$$f(x) = 1 - \frac{1}{2x^2} \left[1 - e^{-2x \cos \theta_c} (1 + 2x \cos \theta_c) \right] \quad (4.25)$$

θ_c is the critical angle, measured from the radial direction, which an ion must have to just miss the aerosol particle, determined by:

$$\sin \theta_c = \frac{b_c}{\delta} \quad (4.26)$$

where:

$$b_c^2 = (s_0 a)^2 \left[1 - \frac{\phi(s_0 a) - \phi(\delta)}{kT} \right] \quad (4.27)$$

Outside the sphere of radius $(\delta + \lambda)$ diffusion - mobility theory holds. Hoppel showed that the total flux of ions to the aerosol particle from this outside region is given by:

$$I = \frac{4\pi D \left[n_0 - n e^{\frac{\phi(r)}{kT}} \right]}{\int_r^\infty \frac{e^{\frac{\phi(r)}{kT}}}{r^2} dr} \quad (4.28)$$

as derived from the diffusion - mobility equation (4.1), and using the condition that the ion density at a large distance from the aerosol particle is n_0 . He then matched the diffusion - mobility

solution to the inner conditions given by I_δ and obtained the following expression for the attachment coefficient:

$$\eta_\delta = \frac{F_\delta}{e^{\phi(\delta+\lambda)/kT} + \frac{F_\delta}{4\pi Da} \int_{\frac{\delta+\lambda}{a}}^{\infty} \frac{1}{x^2} e^{\phi(ax)/kT} dx} \quad (4.29)$$

where $F_\delta = \pi\delta^2\bar{c} f(x)$. Equation (4.29) is valid for $\delta > s_0 a$. If $s_0 a > \delta$, then $\eta_{s_0 a}$ is obtained by replacing δ by $s_0 a$ and F_δ becomes:

$$F_{s_0 a} = \pi a^2 \bar{c} (E.F.) \quad (4.30)$$

where the E.F. here refers to the values computed by Keefe et al. (1968) in the image capture theory. The value of \bar{c} was evaluated from:

$$\bar{c} = \sqrt{\frac{8kT}{\pi m_{ion}}} \quad (4.31)$$

and with an ionic mass of 150 a.m.u. and a temperature of 298K, $\bar{c} = 2.01 \times 10^4 \text{ cm sec}^{-1}$.

Hoppel calculated values of the combination coefficients η_0 , η and η^{12} (using the Keefe and Nolan notation) for different radii using equation (4.29). Under equilibrium conditions it can be shown that:

$$b = \frac{2\eta_0 \left[1 + \frac{\eta^{12}}{\eta} \right]}{1 + 2\frac{\eta_0}{\eta}} \quad (4.32)$$

neglecting the effect of triply charged aerosol particles. The variation of b with radius can now be evaluated using Hoppel's values of η_0 , η , and η^{12} , and the results for this are given in chapter 5. Values of b versus radius from Keefe and Nolan (1962) are also shown. Values of η_0 versus radius from Bricard (1962), Keefe and Nolan (1962) and Hoppel (1974) are presented and compared with the experimental results.

CHAPTER 5.

THE EXPERIMENTAL RESULTS OF b AND η_0 VERSUS RADIUS COMPARED WITH VARIOUS THEORETICAL MODELS.

5.1 Experimental Results.

Tables 5.1 and 5.2 show the results of all the b and η_0 measurements made at different radii. These measurements are plotted graphically in figures 5.1 and 5.2. Two sets of b versus radius experiments were carried out: the first set corresponds to runs where only the combination coefficient b was evaluated, and the second set corresponds to runs where both b and η_0 were determined. The run numbers are tabulated in chronological order. The experimental procedure used for both these sets of measurements is given in section 3.5.

Figure 5.1 illustrates the wide variation in b values obtained. The values tabulated in table 5.2 seem to follow a more linear trend. Two parameters are considered to be responsible for the fluctuation in b values; n_0 , the initial concentration of small ions, and Z , the concentration of the aerosol particles. n_0 here refers to the initial concentration of ions into the mylar vessel, before setting the time $t = 0$ (for $n_{t=0} = 4000$ ions per cm^3). This initial concentration was probably of the same order as the particle concentration for Z less than or equal to approximately 15,000 particles per cm^3 . This initial concentration of ions could be reduced in two ways: (1) by having a high concentration of aerosol particles, Z , which would 'quench' the

Table 5.1 Variation of b with Radius.

Run no.	Geometric mean size of aerosol particles. (10^{-6} cm).	Concentration of aerosol particles. (cm^{-3}).	b ($10^{-6} \text{ cm}^3 \text{ sec}^{-1}$).
1	0.52	15460	0.34 (± 0.04)
2	0.70	10870	0.55 (± 0.06)
3	0.41	12900	0.35 (± 0.04)
4	0.44	16190	0.36 (± 0.04)
5	0.45	19850	0.43 (± 0.05)
6	0.42	15010	0.37 (± 0.04)
7	0.51	18580	0.48 (± 0.06)
8	1.39	24000	0.67 (± 0.07)
9	2.00	17280	1.16 (± 0.15)
10	2.30	12500	2.24 (± 0.29)
11	2.40	9130	3.07 (± 0.41)
12	1.72	26070	1.34 (± 0.16)
13	2.02	13810	2.46 (± 0.27)
14	0.77	29400	0.61 (± 0.08)
15	0.95	13620	1.10 (± 0.16)
16	1.05	11160	1.57 (± 0.21)

TABLE 5.2. Variation of b and η_0 with radius

Run No.	Size (10^{-6} cm)	Concentration of aerosol particles (cm^{-3})	$\frac{N_0}{N}$	f	$\left(\frac{N_0}{N}\right)_{\infty} = \lambda$	b ($10^{-6} \text{ cm}^3 \text{ sec}^{-1}$)	η_0 ($10^{-6} \text{ cm}^3 \text{ sec}^{-1}$)
17	1.49	26040	5.01	0.75	6.67	0.58 (± 0.06)	0.35 (± 0.04)
18	2.65	41320	1.88	0.68	2.76	1.21 (± 0.15)	1.01 (± 0.13)
19	4.00	22310	1.40	0.78	1.79	2.24 (± 0.22)	2.39 (± 0.13)
20	4.17	12160	3.68	2.16	1.70	2.06 (± 0.27)	1.95 (± 0.25)
21	1.26	9310	12.77	1.27	10.05	0.50 (± 0.06)	0.33 (± 0.04)
22	2.29	25540	4.88	1.48	3.30	0.94 (± 0.11)	0.79 (± 0.09)
23	2.43	21250	4.33	1.41	3.08	1.10 (± 0.16)	0.94 (± 0.09)
24	2.68	13220	4.10	1.53	2.68	1.13 (± 0.11)	1.02 (± 0.10)
25	2.12	37730	2.16	0.59	3.68	1.19 (± 0.14)	0.86 (± 0.10)
26	2.31	30350	2.08	0.63	3.28	1.36 (± 0.18)	1.03 (± 0.13)

FIG. 5.1 VARIATION OF b WITH RADIUS

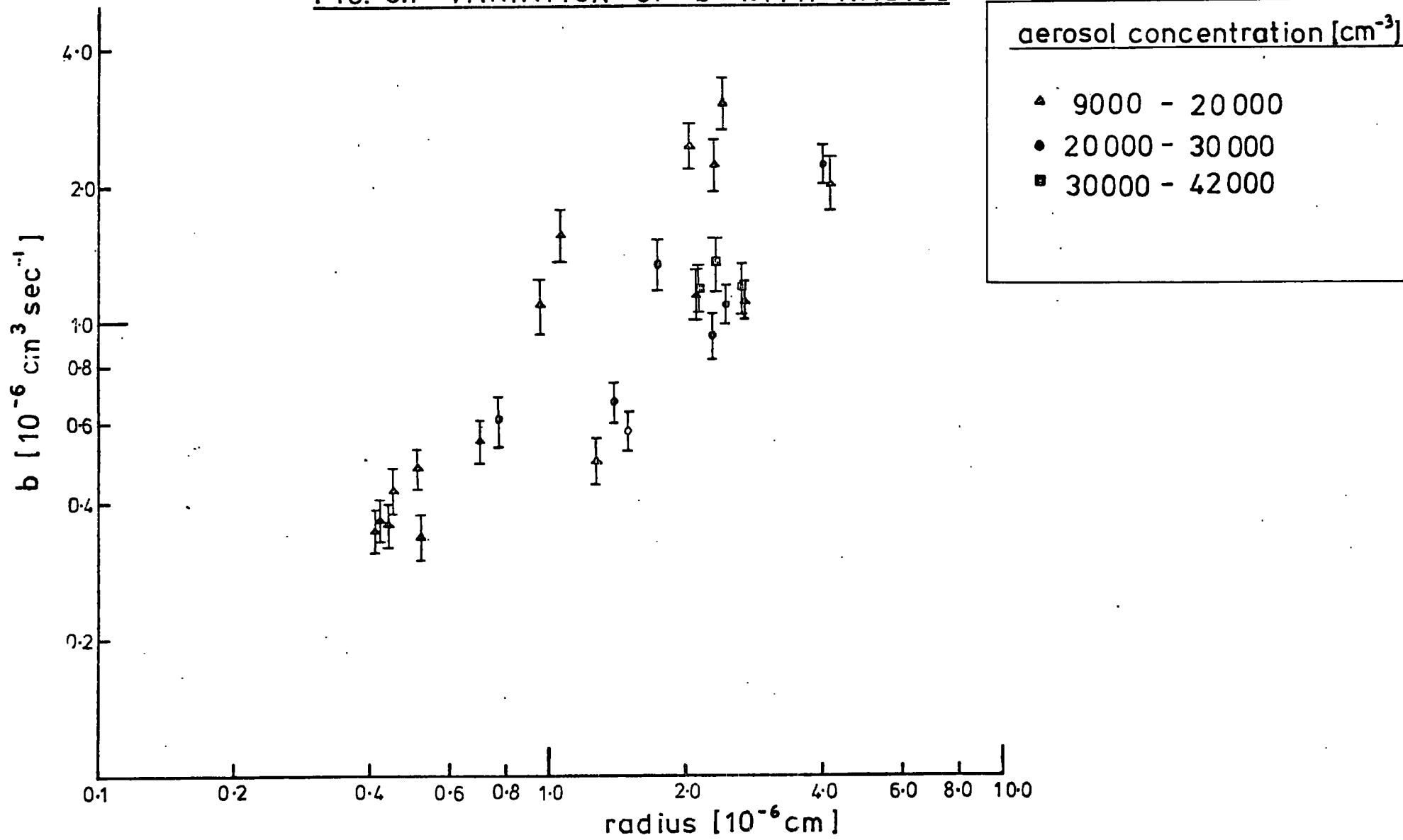
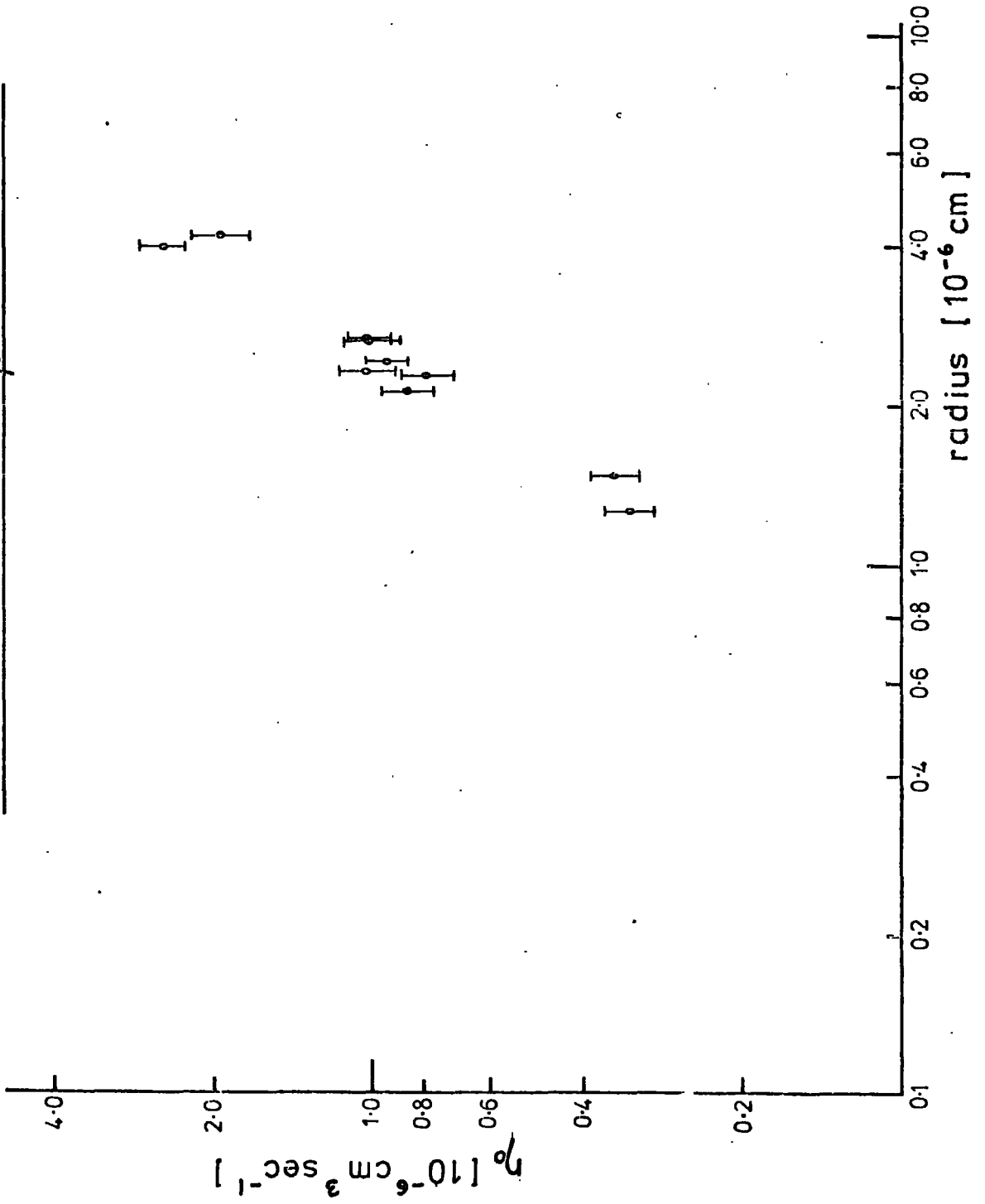


FIG. 5.2 VARIATION OF η_0 WITH RADIUS



high flux of ions, and (2) by careful manipulation of the air supply to the needle in the ion source. These two constraints were in general applied to the second set of runs which are hence more representative of conditions found naturally in the atmosphere. The variation of b with concentration of aerosol particles is shown in the diagram by the symbols on each experimental point. Larger values of Z tended to give the smaller values of b , but this variation also depended on n_0 , which was not recorded since this would have required rapid changing of the sensitivity scale of the electrometer just before each decay.

5.2 Comparison with Other Experimental Results.

The variation of small ion concentration with time in the presence of artificial nuclei in a sealed room has been examined by Burke and Dalu (1969). They found that values of the combination coefficient, b , deduced by Keefe and Nolan (1962) for equilibrium conditions, depended on the nucleus concentration, which mainly controlled the ionic concentration. However, experimental values of combination coefficient b were not determined.

Flanagan (1966) describes two series of measurements of b versus radius. Small ions were produced in a tetrahedral vessel of aluminium walls by having Cobalt 60 sources in the vicinity. The ionization rate could be varied according to the position of the sources. Aerosol particles were produced by passing filtered air over glowing nichrome wire and also by bubbling filtered air through water, for a larger size range of particles. The radius of the particles was measured by the diffusion battery method.

In the first series of experiments the ionic concentration (n) was measured for different aerosol particle concentrations (Z) and the ionization rate kept constant. The vessel was filled with aerosol particles and both Z and n were measured. Filtered air was then pumped in and new values of Z and n were recorded. This process was continued until the vessel contained no aerosol particles. The size of the particles was measured during the run, and the ionization rate determined by measuring the ionic concentration in filtered air both before and after the run. b was evaluated by plotting n versus Z and calculating $Zn/(q - n^2)$ for each point and then taking the average.

In the other series of experiments the ionization rate (q) was varied by the positioning of various Co_{60} sources near the balloon. The ionization rate produced by each source had been measured in a separate set of experiments. The concentration, Z and size of the aerosol particles in the vessel were first measured, and then n was determined for different values of q . Then Z and size were again measured after a necessarily long time lapse and the mean of the two measurements was used for each run. n was plotted against q and b was calculated from the linear relationship $q = bZn$ in the region $n = 0$ to 1000 ions cm^{-3} , (neglecting the n^2 term). Table 5.3 on the following page summarises the results of the two series of experiments. These results compare fairly well with the lower values of b presented in figure 5.1. The accuracy of Flanagan's radii measurements are queried, for the length of time necessary for each run should allow for noticeable coagulation of the particles within the vessel. Flanagan in the second series of experiments was required to make seven separate

measurements of the ionic concentration for different ionization rates before he could obtain a second value of the particle radius.

Table 5.3 Results of Flanagan (1965).

Radius. (10^{-6} cm).	Z (cm^{-3}).	q ion pairs. $\text{cm}^{-3}\text{sec}^{-1}$	b ($10^{-6}\text{cm}^3\text{sec}^{-1}$)
3.46	0 - 25,000	6.6	1.89 (± 0.12)
3.49	0 - 33,000	12.6	2.26 (± 0.12)
5.83	0 - 11,000	4.7	3.13 (± 0.17)
0.53	130,000	0 - 120	0.15 (± 0.01)
0.68	60,000	"	0.50 (± 0.02)
1.41	32,400	"	0.76 (± 0.03)
1.57	12,610	"	0.81 (± 0.04)
1.67	9,593	"	1.00 (± 0.06)
2.57	13,330	"	1.65 (± 0.07)
3.43	27,070	"	2.05 (± 0.10)
4.31	4,321	"	2.36 (± 0.10)

5.3 Theoretical models for b versus radius.

Table 5.4 shows values of b for different aerosol radii computed from Hoppel (1974) compared with values given by Keefe and Nolan (1962). Hoppel's values were evaluated using equations (4.29) to (4.32) with an ionic mass of 150 a.m.u., a mean free path, λ , of 2.1×10^{-6} cm, and mean ion velocity, \bar{c} , of 2.0×10^4 cm sec $^{-1}$. Values

of the trapping distances used are given in chapter 4. Keefe and Nolan's b values were obtained from the variation of η_0 with radius according to equation (4.10) by applying the Boltzmann equilibrium condition:

$$\frac{b}{\eta_0} = \frac{1 + \frac{1}{\ell^2} + \frac{1}{\ell^6} + \frac{1}{\ell^{12}} + \dots}{522\sqrt{a}} \quad (5.1)$$

where $\ell = \exp(\frac{e^2}{2akT})$. This expression takes account of multiple charged nuclei. For these b values the small ions were considered as a cluster of eleven water molecules, following the suggestions of Wright (1936). A value of $1.76 \times 10^4 \text{ cm sec}^{-1}$ was then used for \bar{c} , and $6 \times 10^{-6} \text{ cm}$ for λ .

Table 5.4. Theoretical models for b versus radius.

Radius. (10^{-6} cm).	b (Hoppel) ($10^{-6} \text{ cm}^3 \text{ sec}^{-1}$).	b (Keefe and Nolan) ($10^{-6} \text{ cm}^3 \text{ sec}^{-1}$).
0.2	0.037	-
0.4	0.103	-
0.6	0.179	-
0.8	0.261	-
1.0	0.343	0.355
2.0	0.740	0.790
4.0	1.72	1.77
6.0	2.82	2.86
8.0	-	4.00
10.0	5.00	-

These two sets of theoretical values lie slightly below the lower experimental values of b on figure 5.1. An investigation was

made into the effect of increasing the value of α in Hoppel's theoretical model from 1.4 to 2.4×10^{-6} , which was obtained experimentally in chapter 2. This involved extrapolating the 150a.m.u. curve in figure 4.2 so that the ion-ion trapping distance, d could be obtained for $\alpha = 2.4 \times 10^{-6}$. This gave a value of $d \doteq 4.5 \times 10^{-6}$ cm. Calculations of the combination coefficient η were then made using Hoppel's method (chapter 4), for aerosol particle radii of 0.4, 1.0 and 4.0×10^{-6} cm. An ionic mass of 150 a.m.u. was used, as indicated above, and Hoppel's value for \bar{c} was used. The mean free path used was 1.2×10^{-6} cm, which was evaluated from the experimental value of the mobility (chapter 2), using equation (1.5), with $m_{ion} = 150$ a.m.u. and $M_{molecule} = 28.8$ a.m.u. The integral in the denominator of equation (4.29) was solved numerically on the computer for each aerosol radius chosen using the Romberg iteration method. Values of η calculated for the 0.4, 1.0 and 4.0×10^{-6} cm cases were bigger than the corresponding values calculated by Hoppel by factors of 1.84, 1.68 and 1.08 respectively. However, since b is determined from:

$$b = \frac{2 \eta_0 \left[1 + \frac{\eta^{12}}{\eta} \right]}{1 + 2 \frac{\eta_0}{\eta}} \quad (5.2)$$

and only the coefficient η is affected by the change in α (as η_0 and η^{12} are not evaluated on the basis of 3-body trapping theory), the net increase in b for the three radii is only of the order of: 3%, 9% and 3% respectively. This does not account for the discrepancy between the lower experimental b values and theoretical values. The uncertainty in the values of m_{ion} , λ , and \bar{c} are the more likely causes of difference. For example, Hoppel (1974) showed that decreasing the ionic mass from 150 to 60 a.m.u. would increase η_0 by upto 50%,

and increase η by 15% for particle radii less than 4×10^{-6} cm. If one assumes a similar percentage increase for η^{12} , it can be shown that the value of b is increased by 46%, 41% and 30% for particle radii of 0.4, 1.0 and 4.0×10^{-6} cm respectively.

Unfortunately the theoretical models for the calculation of attachment coefficients between ions and nuclei do not take into account the relative concentrations of n_0 and Z , so a direct comparison of the experimental and theoretical values of b is difficult for the larger values of b obtained.

5.4 Comparison of η_0 versus Radius Values with Theory.

Figure 5.2 shows a plot of all the experimentally determined values. It was impossible to obtain values of η_0 for radius, $a < 1.0 \times 10^{-6}$ cm by this method, since in this case the relative number of charged particles is less than 11% of the total particle concentration and is therefore approaching the limiting accuracy of the photo-electric counter. As shown in table 5.2 these η_0 values were all evaluated from the second set of b versus radius runs. Theoretically calculated values computed from Bricard (1962), Keefe and Nolan (1962), and Hoppel (1974) are given in table 5.5. The values of m_{ion} , λ and \bar{c} used by Keefe and Nolan and Hoppel are discussed in the previous section. Bricard used a value of 1.3×10^{-6} for λ , based on the Langevin expressions for diffusion and mobility, (given in chapter 1). He assumed that small ions are single molecules with either an extra electron or with an electron missing, and that $m_{ion} \approx m_{molecule}$, with $\bar{c} = 4.59 \times 10^4$ cm sec⁻¹. This is contrary to

the idea of a small ion consisting of a cluster of molecules. The η_0 values from Bricard are computed from equations (4.2) and (4.6). They are noticeably smaller than the other two sets of η_0 values given, mainly due to the fact that the image force term has been neglected in this derivation.

Table 5.5 Theoretical Models for η_0 versus Radius.

Radius. (10^{-6} cm).	(Bricard) (10^{-6} cm ³ sec ⁻¹)	(Keefe and Nolan) (10^{-6} cm ³ sec ⁻¹)	(Hoppel) (10^{-6} cm ³ sec ⁻¹)
0.2	0.0057	-	0.019
0.4	0.022	-	0.056
0.6	0.049	-	0.1202
0.8	0.083	-	0.157
1.0	0.124	0.197	0.218
2.0	0.396	0.553	0.575
4.0	1.099	1.48	1.40
6.0	1.886	2.54	2.25
8.0	-	3.65	-
10.0	-	-	3.98

The experimental points give fairly good agreement with Keefe and Nolan's and Hoppel's η_0 values. As with the b versus radius results, the theoretical values are somewhat lower: the mass, mean velocity and mean free path of the ions could again account for this.

5.5 Conclusion.

The comparison between the experimental results and theory indicates that the technique adopted here for measuring combination coefficients η_0 and b with radius is satisfactory providing careful control is applied on the initial ion concentration entering the mylar vessel. The higher b values obtained indicate that theories for calculating the attachment coefficients could require modification in conditions of high ionization, or when the ionic concentration is of the same order as the particle concentration. Finally, agreement needs to be sought on the values of n , \bar{c} and λ of the small ions before experimental and theoretical results can be accurately compared.

*

*

*

REFERENCES.

- Bricard, J. (1949) L'équilibre Ionique de la Basse Atmosphère. J. Geophys. Res., 54, 39-52.
- Bricard, J. (1962) La Fixation des Petits Ions Atmosphériques sur les Aérosols Ultra-fins. Geofis. Pura e Appl., 51, 237-242.
- Bricard, J. (1965) Action of Radioactivity and of Pollution upon Parameters of Atmospheric Electricity. pp 82-107, "Problems of Atmospheric and Space Electricity", (Ed. Coronti). Elsevier, London.
- Burke, T.P. and Dalu, G. (1969) Capture of Small Ions by Particles. pp 177-183, "Planetary Electrodynamics" Vol. 1. (Ed. Coronti and Hughes.) Gordon and Breach, New York, London, Paris.
- Chalmers, J.A. (1967) "Atmospheric Electricity". 2nd Ed., Pergamon Press, London.
- Coulier, P.J. (1875) Note sur une Nouvelle Propriété de L'air. J. Pharm. Chim., 22, 254.
- Flanagan, V.P.V. (1965) "Aerosols and the Ionization Balance of the Atmosphere". Ph.D. Thesis, Cambridge Univ.
- Flanagan, V.P.V. (1966) Measurements of the Coefficients of Combination of Small Ions with Aerosol Particles. Pure Appl. Geophys., 64, 197-203.

- Flanagan, V.P.V. and Tayler, P. Tables of Aerosol Physics Functions; Mobility and Falling Speed of Spheres. (1967). Atmos. Environ., 1, 327-340.
- Fuchs, N.A., Stechkina, I.B. and Starosseleskii, V.I. On the Determination of Particle Size Distribution in Polydisperse Aerosols by the Diffusion Method. (1962). B. J. Appl. Phys., 13, 280-281.
- Gunn, R. (1954). Diffusion Charging of Atmospheric Droplets by Ions, and the Resulting Combination Coefficients. J. of Meteorology, 11, No.5, 339-347.
- Hoppel, W.A. (1969). Application of Three-body Recombination and Attachment Coefficients to Tropospheric Ions. Pure and Appl. Geophys., 75, 158-166.
- Hoppel, W.A. (1974). Ion-aerosol Attachment Coefficients and the Diffusional Charging of Aerosols. Proc. 5th International Conference in Atmospheric Electricity, Garmisch-Partenkirchen, September 1974. "Atmospheric Electricity". Vol. 1. (English Edition). Israel Program for Scientific Translations, Jerusalem.
- Israel, H. (1971). Charge Equilibrium in Aerosols According to the Boltzmann Distribution Law. Proc. Roy. Irish Acad., 60, Sect.A, 27-45.
- Keefe, D., Nolan, P.J. and Rich, T.A. (1959). Influence of Image Forces on Combination in Aerosols. Geofis. Pura e Appl., 50, 155-160.

- Keefe, D. and Nolan, P.J. (1962). Combination Coefficients of Ions and Nuclei. Proc. Roy. Irish Acad., 62, Sect.A, 43-53.
- Keefe, D., Nolan, P.J. and Scott, J.A. (1968). Influence of Coulomb and Image Forces on Combination in Aerosols. Proc. Roy. Irish Acad., 66, Sect.A, 17-29.
- Kennard, E.H. (1938). "Kinetic Theory of Gases". McGraw.
- DeMarcus, W.C. and Thomas, J.W. (1952). O.R.N.L. Report 1413. (available from Office of Technical Services, Dept. of Commerce, Washington D.C.).
- Megaw, W.J. and Wiffen, R.D. (1963). Measurement of the Diffusion Coefficient of Homogeneous and Other Nuclei. J. de Rech. Atmos., 1, 113-125.
- Megaw, W.J. and Wiffen, R.D. (1964). Aerosols, Physical Chemistry and Applications, Czechoslovak Academy of Sciences.
- Metnieks, A.L. and Pollak, L.W. (1961). Tables and Graphs for Use in Aerosol Physics. Part II. Inst. Adv. Studies, Dublin, Geophysical Bulletin No. 20.
- Millikan, R.A. (1923). Phys. Rev. 22 (2nd s.), 1.
- Natanson, G.L. (1959). The Theory of Volume Recombination of Ions. Zh. Techn. Fiz. 29, 1373-1380.
- Nolan, J.J. and Guerrini, V.H. (1935). The Diffusion Coefficients and Velocities of Fall in Air of Atmospheric Nuclei. Proc. Roy. Irish Acad. 43(A2), 5.
- Nolan, J.J., Nolan, P.J. and Gormley, P.G. (1938). Diffusion and Fall of Atmospheric Nuclei. Proc. Roy. Irish Acad., 45A, 47-63.

- Nolan, P.J. (1943). The Recombination Law for Weak Ionization. Proc. Roy. Irish Acad., 49A, 67-90.
- Nolan, P.J. and Pollak, L.W. (1946). The Calibration of a Photo-electric Nucleus Counter. Proc. Roy. Irish Acad., 51(A2), 9-31.
- Nolan, P.J. and Kennan, E.L. (1949). Condensation Nuclei from Hot Platinum; Size, Coagulation Coefficient and Charge Distribution. Proc. Roy. Irish Acad., 52, 171-190.
- Nolan, P.J. and Kuffel, E. (1957). Metal Point Discharge Nuclei and the Production of Multiply Charged Ions from Condensation Nuclei. Geofis. Pura e Appl., 36, 201-210.
- Nolan, P.J. and O'Toole, C.P.J. (1959). The Condensation Nuclei Produced by Point Discharge. Geofis. Pura e Appl., 42, 117.
- O'Connor, T.C. and Roddy, A.F. (1966). The Production of Condensation Nuclei by Heated Wires. J. Rech. Atmos., 2, 239-244.
- Pollak, L.W. and Metnieks, A.L. (1957). On the Determination of the Diffusion Coefficient of Heterogeneous Aerosols by the Dynamic Method. Geofis. Pura e Appl., 37, 183-190.
- Pollak, L.W. and Metnieks, A.L. (1959). The Influence of Air-flow on the determination of the Diffusion Coefficient of Heterogeneous Aerosols by the Dynamic Method. Geofis. Pura e Appl., 44, 224-232.

- Rich, T.A. (1959). The Average Size of Submicron Aerosol Particles. Intern. Journ. Air Pollution; 1, 288-292.
- Smolukowski, M. (1918). Z. Phys. Chem., 92, 129.
- Torreson, O.W. (1939). Condensation Nuclei in the Atmosphere of Peru, and their Relation to Atmospheric-Electrical and Meteorological Observations. Terr. Magn. Atmos. Elect. 44, 59-74.
- Townsend, I.S. (1900). The Conductivity Produced in Gases by the Motion of Negatively Charged Ions. Nature, 62, 340-341.
- Wasser, V.E. (1933). Physik. Z. 34, 257.
- Whitby, K.T. and McFarland, A.R. (1961). The Decay of Unipolar Small Ions and Homogeneous Aerosols in Closed Spaces and Flow Systems. Int. Conf. Ionization of the Air. Philadelphia: Franklin Inst. 7, 1-23.
- Wright, H.L. (1936). The Size of Atmospheric Nuclei: Some Deductions from Measurements of the Number of Charged and Uncharged Nuclei at Kew Observatory. Proc. Phys. Soc., 48, 675-689.

*

*

*

ACKNOWLEDGEMENTS.

I wish to express my gratitude to all those who have given help during the course of this work. In particular, I should like to thank my supervisor, Dr. S.G.Jennings, for continual support and useful advice during my course at Durham.

I am also very grateful for the help given in the construction of various parts of the apparatus by Mr J.Moralee, and for Mr P.Roe's help with the photographs.

Finally I should like to thank my fiancée, Rachel, who has encouraged and supported me in this work at all times.

This work was sponsored by the U.S. Army, European Research Office under research contract No. DAJ-A37-75-C-1913.

*

*

*